symmetry

IMPACT FACTOR 2.2

CITESCORE 5.4

Review

Lepton Flavor Universality Tests in Semileptonic $b \to c$ Decays

Suzanne Klaver and Marcello Rotondo

Special Issue

Symmetries and Anomalies in Flavour Physics

Edited by

Dr. Stefania Ricciardi, Dr. Thomas Blake and Dr. Farvah Nazila Mahmoudi

MDPI

https://doi.org/10.3390/sym16080964

symmetry

MDPI

Review

Lepton Flavor Universality Tests in Semileptonic $b \to c$ Decays

Suzanne Klaver [1,2,*] **and Marcello Rotondo** [3,*]

[1] Nikhef National Institute for Subatomic Physics, Science Park 105, 1098 XG Amsterdam, The Netherlands
[2] Faculty of Science, Vrije Universiteit Amsterdam, De Boelelaan 1105, 1081 HV Amsterdam, The Netherlands
[3] INFN, Laboratori Nazionali di Frascati, Via Enrico Fermi 54, 00044 Frascati, Italy
* Correspondence: suzanne.klaver@cern.ch (S.K.); marcello.rotondo@cern.ch (M.R.)

Abstract: Semileptonic decays of b- to c-hadrons provide an exciting environment to probe new physics and currently present some of the most compelling anomalies in the field of flavor physics. Measurements of the lepton flavor universality ratios $\mathcal{R}(D^{(*)})$, comparing branching fractions with τ and μ leptons, show a discrepancy of over 3σ with respect to the Standard Model, and suggest that the coupling to τ leptons is stronger than predicted. Measurements of angular distributions as well as polarization in b- to c-hadron decays provide additional sensitivity to new physics. This review article offers an overview of the theory of semileptonic b- to c-hadron decays, presents the experiments and experimental techniques used to perform measurements of these decays, and summarizes the latest experimental results with their implications.

Keywords: semileptonic decays; flavor physics; lepton universality; B physics

check for updates

Citation: Klaver, S.; Rotondo, M. Lepton Flavor Universality Tests in Semileptonic $b \to c$ Decays. *Symmetry* **2024**, *16*, 964. https://doi.org/10.3390/sym16080964

Academic Editor: Francesco Renga

Received: 1 July 2024
Revised: 19 July 2024
Accepted: 22 July 2024
Published: 29 July 2024

1. Introduction

The Standard Model (SM) of particle physics is a well-established theoretical framework that describes the fundamental particles and their interactions. It classifies all known subatomic particles into two groups: fermions, which are the building blocks of matter, and bosons, which mediate the fundamental forces. A key assumption within the SM is lepton flavor universality (LFU). This principle states that the interactions of leptons (electrons, muons, and tau particles) are identical except for differences due to their masses. This assumption leads to predictions about the rates and kinematics of particle decays involving different kinds of leptons.

The study of b hadrons provides a unique window into the fundamental interactions that govern particle physics. Of particular interest are semileptonic decays of B mesons, like $\overline{B} \to D^{(*)}\ell\nu_\ell$ decays, where $\ell = e, \mu$ or τ leptons. These processes, involving a transition from a B meson to a D meson (or its excited states) accompanied by a lepton and a neutrino, are probes which are sensitive to the SM and potential new physics. The inclusion of charge-conjugate decay modes is implied. Throughout the paper, the signs conventions apply to $b \to c$, and can be extended to $\overline{b} \to \overline{c}$ transitions with proper sign change.

The semileptonic decays involving a τ lepton, usually called semitauonic decays, are of special interest. These decays are mediated in the SM by the charged-current weak interaction, where the underlying quark transition $b \to c\tau\nu_\tau$ is governed by the exchange of a W boson. The rates and distributions of these decays can precisely be predicted within the SM framework. However, experimental results from BABAR, Belle, and LHCb have shown deviations from these SM predictions. These anomalies are observed by measurements of the ratios $\mathcal{R}(D)$ and $\mathcal{R}(D^*)$, defined as the following ratio of branching fractions:

$$\mathcal{R}(D) = \frac{\mathcal{B}(\overline{B} \to D\tau\nu_\tau)}{\mathcal{B}(\overline{B} \to D\ell\nu_\ell)}, \qquad \mathcal{R}(D^*) = \frac{\mathcal{B}(\overline{B} \to D^*\tau\nu_\tau)}{\mathcal{B}(\overline{B} \to D^*\ell\nu_\ell)}, \tag{1}$$

where ℓ represents either an electron or a muon. The world average values of the existing measurements of $\mathcal{R}(D)$ and $\mathcal{R}(D^*)$ exceed the SM prediction by about three standard

deviations. This deviation has led to considerable theoretical interest and prompted a wide range of hypotheses to explain the anomalies. See Refs. [1,2] for previous reviews on LFU tests with semileptonic decays, and Refs. [3,4] for general reviews of theory and experimental techniques for semileptonic b-hadron decays.

We begin this review with an overview of the semileptonic decays in the SM in Section 2. In Section 3, we provide an overview of the experimental techniques essential to perform semileptonic decays at B factories and at LHCb. In the following section, Section 4, we report a summary of the measurements of the $\mathcal{R}(H_c)$ ratios obtained at B factories and at the LHC. We focus the short descriptions of the analyses on a few key points. We also describe additional measurements beyond the $\mathcal{R}(H_c)$ ratios that could have significant impact with larger datasets. In Section 5, we show the world average for $\mathcal{R}(D)$ and $\mathcal{R}(D^*)$ as obtained by the HFLAV collaboration and discuss its implications. In the last section, Section 6, we briefly explore the near future of LFU searches.

2. Semileptonic Decays and Lepton Flavor Universality

Semileptonic decays of b hadrons (H_b) are well understood in the framework of the SM. At the lowest order, $H_b \to H_c \ell \nu_\ell$ decays proceed through the electroweak transition $b \to c \ell \nu_\ell$, as illustrated in Figure 1. These processes are theoretically described by the electroweak effective Hamiltonian,

$$\mathcal{H}_{\text{eff}} = \frac{4G_F}{\sqrt{2}} V_{cb} (\bar{c}\gamma_\mu P_L b)(\bar{\ell}\gamma^\mu P_L \nu_\ell), \tag{2}$$

where, as usual, spinors are represented by their corresponding particle symbols (the corresponding adjoint fields are represented with the overlined particle name), $P_L = (1 - \gamma_5)/2$, G_F is the Fermi constant, V_{cb} is an element in the CKM matrix, and the W-boson is integrated out at tree level exploiting the $m_b \ll m_W$ hierarchy. A crucial feature of semileptonic decays is that the leptonic current and the hadronic part factorize in the matrix element. As consequence, the decay amplitude for $H_b \to H_c \ell \nu_\ell$ takes the following form [5,6]:

$$\mathcal{M}(H_b \to H_c \ell \nu_\ell) \propto V_{cb} L^\mu \langle H_c | \bar{c}\gamma_\mu P_L b | H_b \rangle, \tag{3}$$

where L^μ is the leptonic current. The QCD corrections are fully included in the hadronic matrix element $\langle H_c | \bar{c}\gamma_\mu P_L b | H_b \rangle$. A small violation of this factorization is due to the QED corrections arising from, for example, photon exchange between quark and leptons. These are assumed to be small and added as corrections to the decay amplitude.

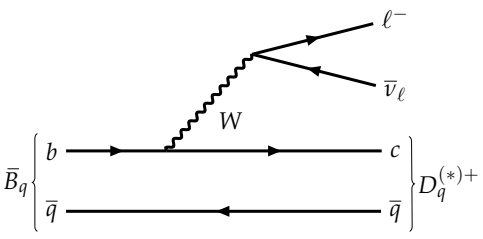

Figure 1. Diagram of the $\overline{B}_q \to D_q^{(*)+} \ell^- \overline{\nu}_\ell$ decay for the SM process mediated by vector boson W.

The hadronic matrix element can be parameterized in terms of form factors, which are non-perturbative functions of the momentum transferred by the lepton system, $q^2 = (p_{H_b} - p_{H_c})^2 = (p_\ell + p_{\nu_\ell})^2$, where p_i are the four-momenta of the particles considered. In the following, we briefly describe the exclusive semileptonic $\overline{B} \to D \ell \nu_\ell$ decays as an example. The hadronic matrix element in Equation (3) for $B \to D$ transitions (where only pseudoscalar mesons are involved) becomes

$$\langle D | \bar{c}\gamma^\mu b | B \rangle = f_+(q^2) \left(p_B^\mu + p_D^\mu - \frac{m_B^2 - m_D^2}{q^2} q^\mu \right) + f_0(q^2) \frac{m_B^2 - m_D^2}{q^2} q^\mu, \tag{4}$$

where p_B and p_D are the four-momenta of the mesons and the $f_+(q^2)$ and $f_0(q^2)$ are the two relevant form factors. The differential branching fraction for the $\bar{B} \to D\ell\nu_\ell$ decay can be written as [7]

$$\frac{d\mathcal{B}(\bar{B} \to D\ell\nu_\ell)}{dq^2} \propto \tau_B \lambda^{1/2} \left(1 - \frac{m_\ell^2}{q^2}\right)^2 \left[\frac{\lambda}{m_B^4}\left(1 + \frac{m_\ell^2}{2q^2}\right) f_+^2(q^2) + \left(1 - \frac{m_D^2}{m_B^2}\right)^2 \frac{3m_\ell^2}{2q^2} f_0^2(q^2)\right], \quad (5)$$

where $\lambda = \lambda(q^2, m_B, m_D) = (q^2 - m_B^2 - m_D^2)^2 - 4m_B^2 m_D^2$, τ_B is the B meson lifetime, and the constant of proportionality is $\eta_{EW} G_F^2 |V_{cb}|^2 m_B / 192\pi^3$. Factor η_{EW} takes into account the short-distance EW corrections, and is known well to be $\eta_{EW} \approx 1.0066$ [8]. For the case of light leptons, $\ell = e, \mu$, the contribution from $f_0(q^2)$ in Equation (5) becomes negligible because it is suppressed by m_ℓ^2/q^2 while it is relevant for decays into τ leptons.

The predictions for the $\bar{B} \to D\ell\nu_\ell$ branching fraction for various kind of leptons are determined by integrating Equation (5) over the q^2 ranges from $q^2_{min} = m_\ell^2$ to $q^2_{max} = (m_B - m_D)^2$. This requires knowledge of form factors $f_{0,+}(q^2)$. There are various theoretical approaches to compute the form factors. For a detailed review, see Ref. [2]. Among the various methods, lattice QCD (LQCD) and light-cone sum rules (LCSR) are the most frequently used. For the $\bar{B} \to D\ell\nu_\ell$ decay, there are many LQCD results available at zero recoil, where the hadron in the final state is in the b-hadron rest frame. Modern LQCD results are obtained beyond zero recoil; see Refs. [9–11]. The calculations based on LCSR are valid in the region of negative q^2 and are assumed to be valid in the physical region of small q^2 (large recoil). In general, the extrapolation to the full q^2 range requires a proper parameterization. In the past, the commonly used parameterization was the one formulated in Ref. [12] (CLN), but at present, only the less model-dependent parameterizations from Ref. [13] (BGL) and Ref. [14] (BCL) are used.

The lepton flavor universality can be probed by calculating the ratio of branching fractions between light leptons ($\ell = e, \mu$) and τ. This ratio can be written in general for any b hadron (H_b) decaying semileptonically into a c hadron (H_c) as

$$\mathcal{R}(H_c) = \frac{\mathcal{B}(H_b \to H_c \tau \nu_\tau)}{\mathcal{B}(H_b \to H_c \ell \nu_\ell)}, \quad (6)$$

where the branching ratio in the denominator can be either for $\ell = e$ or $\ell = \mu$, but in some measurements it can represent the average of the branching ratios with $\ell = e$ and $\ell = \mu$.

This ratio is typically used instead of the absolute branching fraction of $H_b \to H_c \tau \nu_\tau$ decays to cancel uncertainties which are common to the numerator and the denominator. These include $|V_{cb}|$ and several theoretical uncertainties on the hadronic current. Also, many experimental reconstruction uncertainties are canceled. Ratio $\mathcal{R}(H_c)$ depends on the mass of the leptons involved and is lesser than unity because of the much higher mass of the τ lepton compared to $\ell = e, \mu$ leptons. It is also affected by the hadronic form factors whose contributions depend on the lepton masses as well, such as $f_0(q^2)$ in the $\bar{B} \to D\ell\nu_\ell$ case. For a vector final state, like the decay $\bar{B} \to D^*\ell\nu_\ell$, both the vector and the axial currents contribute to the hadronic matrix element. In this case, there are four form factors that contribute to the decay. In the limit of zero lepton mass, only three of them are relevant. Detailed calculations can be found in Refs. [4,15].

The theoretical uncertainties on $\mathcal{R}(H_c)$ predictions are dominated by the uncertainties on the form factors. The common form factors, which are relevant independent of the lepton masses, can be extracted from the analysis of the differential rate of $H_b \to H_c \ell \nu_\ell$, with $\ell = e, \mu$. For example, the analyses of the differential rate of $\bar{B} \to D\ell\nu_\ell$ as a function of q^2, carried on by BABAR and Belle, allow determination of the shape of the form factor $f_+(q^2)$ with great precision. For the $\bar{B} \to D^*\ell\nu_\ell$ decays, with D^* decaying into $D\pi$ or $D\gamma$, the determination of the form factors requires a multidimensional analysis. The kinematic variables usually adopted are: q^2, the helicity angles of the D and the lepton ℓ, θ_{hel} and θ_ℓ, respectively, and the angle χ between the hadronic and leptonic two-body decay planes. For $\ell = e, \mu$, these analyses are carried out by BABAR, Belle and Belle II, allowing a precise determination of the three form factors relevant for the massless lepton case.

In Table 1, we report a summary of various predictions of $\mathcal{R}(D)$ and $\mathcal{R}(D^*)$. We do not foray into the details of these calculations. Most of these use both theoretical and experimental inputs for the shape of the form factors of $\bar{B} \to D\ell\nu_\ell$ and $\bar{B} \to D^*\ell\nu_\ell$ decays. While the predictions for $\mathcal{R}(D)$ are consistent for both the central values and uncertainties, there are some differences for $\mathcal{R}(D^*)$. It has been challenged, for example, in Ref. [16], that a pure SM prediction should not use data from semileptonic decays into light leptons to constrain the form factor shape, because there could be new physics affecting these decays as well. While we believe this is in principle correct, at present, the LQCD calculations are not precise enough and are valid only in a limited region of high q^2. Under the assumption that new physics only affects semitauonic decays, the predictions that use both experimental data and LQCD can be considered SM predictions.

Table 1. Predictions for $\mathcal{R}(D^*)$ and $\mathcal{R}(D)$. Some calculations extract simultaneously $\mathcal{R}(D^*)$ and $\mathcal{R}(D)$ from a global fit and also provide correlations, but these are ignored here. The calculation below the HFLAV average are not included in the average but are shown for completeness. In the future, the combination of the SM predictions should be revisited including more recent predictions. The last three predictions for $\mathcal{R}(D^*)$ are based only on LQCD calculations.

Prediction	$\mathcal{R}(D^*)$	$\mathcal{R}(D)$
D. Bigi, P. Gambino [7]		0.299 ± 0.003
P. Gambino, M. Jung, S. Schacht [17]	$0.254^{+0.007}_{-0.006}$	
M. Bordone, M. Jung, D. van Dyk [18]	0.247 ± 0.006	0.298 ± 0.003
F. Bernlochner, et al. [19]	0.257 ± 0.003	0.299 ± 0.003
S. Jaiswal, S. Nandi, S.K. Patra [20]	0.257 ± 0.005	0.299 ± 0.004
BABAR Coll. [21]	0.253 ± 0.005	
G. Martinelli, S. Simula, L. Vittorio [16]		0.296 ± 0.008
Arithmetic average (HFLAV) [22]	$\mathbf{0.254 \pm 0.005}$	$\mathbf{0.298 \pm 0.004}$
D. Bigi, P. Gambino, S. Schacht [23]	0.260 ± 0.008	
M. Bordone, M. Jung, D. van Dyk [18]	0.250 ± 0.003	0.297 ± 0.003
F. Bernlochner, et al. [24]	0.249 ± 0.003	0.288 ± 0.004
FLAG Coll. [25]		0.2951 ± 0.0031
G. Martinelli, S. Simula, L. Vittorio [26]	0.275 ± 0.008	
I. Ray, S. Nandi [27]	0.258 ± 0.012	0.304 ± 0.003
FNAL/MILC, A. Bazavov et al. [9]	0.265 ± 0.013	
HPQCD, J. Harrison, C. Davies [10]	0.273 ± 0.015	
JLQCD, Y. Aoki et al. [11]	0.252 ± 0.022	
G. Martinelli, S. Simula, L. Vittorio [28]	0.262 ± 0.009	
M. Bordone, A. Juttner [29]	$0.262 \pm 0.005 \pm 0.012$	

The FNAL/MILC Collaboration conducted the first unquenched LQCD calculation of the form factors for the $\bar{B} \to D^*\ell\nu_\ell$ transition at non-zero recoil. Their prediction for $\mathcal{R}(D^*)$ is 0.265 ± 0.013 [9]. The HPQCD and JLQCD collaborations have also released their own calculations, with predictions of $\mathcal{R}(D^*) = 0.273 \pm 0.015$ [10] and $\mathcal{R}(D^*) = 0.252 \pm 0.022$ [11], respectively. Combinations of these lattice calculations have recently been performed in Refs. [28,29], and the results are reported in Table 1. It is worth to mention that the results of joint fits between LQCD and experimental data are slightly in tension with these LQCD-only calculations. The result obtained by FNAL/MILC is $\mathcal{R}(D^*) = 0.2492 \pm 0.0012$ [9], while HPQCD obtained $\mathcal{R}(D^*) = 0.2482 \pm 0.0020$ [10]. Moreover, JLQCD predicts a slope for the form factors which is not consistent with FNAL/MILC and HPQCD. Hopefully future calculations will provide higher precision even further from zero recoil, making the various approaches used in the extrapolation to the full range less relevant.

The discussion above for $\bar{B} \to D\ell\nu_\ell$ and $\bar{B} \to D^*\ell\nu_\ell$ decays can be extended to other hadrons and to decays into other excited charm hadron states. A comprehensive summary of existing predictions is shown in Ref. [30]. Here, we just report some of the predictions for semitauonic decay modes that have already been observed.

1. $\Lambda_b \to \Lambda_c \ell \nu_\ell$: measurements of semileptonic Λ_b decays probe different spin structures. The precise predictions of $\mathcal{R}(\Lambda_c) = 0.324 \pm 0.004$ were obtained in Ref. [31], combining LQCD calculations for $\Lambda_b \to \Lambda_c$ form factors beyond zero recoil from Ref. [32] and data available for $\Lambda_b \to \Lambda_c \mu \nu_\mu$ from LHCb [33].
2. $B_c \to J/\psi \ell \nu_\ell$: these decays, with $J/\psi \to \mu^+ \mu^-$, provide a clear experimental signature for LFU tests thanks to the leptons in the final state. The recent LQCD calculation from Ref. [34] provides a high-precision prediction of $\mathcal{R}(J/\psi) = 0.2582 \pm 0.0038$.

In addition to ratios $\mathcal{R}(H_c)$, a wide range of observables for semitauonic b-hadron decays have been extensively analyzed in the literature. These observables could be valuable in further constraining additional operators of new physics models. Of particular interest are the measurements of D^* and τ polarization.

The differential decay rate for $\bar{B} \to D^* \ell \nu_\ell$ decays with $D^* \to D\pi$, integrated over q^2, $\cos\theta_\ell$ and χ is

$$\frac{1}{\Gamma}\frac{d\Gamma}{d\cos\theta_{hel}} \propto F_L \cos^2\theta_{hel} + (1 - F_L)\frac{\sin^2\theta_{hel}}{2}, \tag{7}$$

where $F_L \equiv F_L^{D^*} = \Gamma_{\lambda=0}(\bar{B} \to D^* \ell \nu)/\Gamma(\bar{B} \to D^* \ell \nu)$ is the fraction of the D^* longitudinal polarization (D^* helicity $\lambda = 0$). A similar analysis can be conucted for $\bar{B} \to D^{(*)} \tau \nu_\tau$, followed by the hadronic τ decay in $\tau \to h\nu$. The differential rate as a function of $\cos\theta_h$, where θ_h is the helicity angle of hadron h, can be written as

$$\frac{1}{\Gamma}\frac{d\Gamma}{d\cos\theta_h} = \frac{1}{2} + \alpha_h \frac{P_\tau}{2}\cos\theta_h, \tag{8}$$

where P_τ is the τ polarization and α_h is a constant that depends on the final state. This is $\alpha_h \approx 1$ for a pion, which is the best polarizer, and it decreases with the increasing mass of hadronic state h. Some recent predictions for $F_L^{D^*}$ and P_τ are shown in Table 2. To date, only a few measurements have been conducted, and these are detailed in Section 4.3.

Table 2. Predictions for the τ polarization P_τ and the fraction of the longitudinal D^* polarization $F_L^{D^*}$ for recent LQCD calculations and their combinations reported in the last two rows.

Prediction	$P_\tau(D^*)$	$F_L^{D^*}$
FNAL/MILC, A. Bazavov et al. [9]	-0.529 ± 0.007	0.418 ± 0.009
HPQCD, J. Harrison, C. Davies [10]	-0.547 ± 0.019	0.395 ± 0.024
JLQCD, Y. Aoki et al. [11]	-0.509 ± 0.011	0.448 ± 0.016
G. Martinelli, S. Simula, L. Vittorio [28]	-0.521 ± 0.006	0.425 ± 0.007
M. Bordone, A. Juttner [29]	$-0.522 \pm 0.006^{+13}_{-22}$	$0.424 \pm 0.007^{+21}_{-25}$

3. Experiments and Experimental Techniques

The semileptonic decays of heavy hadrons produce final states with charged tracks or neutral particles, a charged lepton and at least one neutrino. The presence of the neutrino places many challenges for the separation of signal from background and for the reconstruction of the full decay kinematics. The most recent results on b-hadron semileptonic decays come from e^+e^- experiments operating at the $\Upsilon(4S)$ energy and from pp collisions at the Large Hadron Collider (LHC).

Here, we present key features of b-hadron production in different environments which are relevant for understanding the experimental setup and analysis techniques developed to study semileptonic decays.

3.1. General Experimental Techniques

To mitigate the fact that all decays are partially reconstructed decays due to the neutrino, each of the measurements in this paper uses template fits based on Monte Carlo (MC) simulations. These simulations are cross-checked with fully reconstructed control

channels, and data-driven corrections are applied when necessary. The fit variables chosen for the templates are kinematic variables that best distinguish the signal channel from the normalization channel and other backgrounds. One of the most challenging parts of these analyses is obtention of correct MC templates for each of the components. MC samples are often corrected for b hadron kinematics, as well as track occupancy in the detector, using control samples. In addition, the MC samples are reweighted to match different form factors parameterizations.

Common backgrounds to all analyses come from the following sources: partially reconstructed B decays, such as semileptonic decays to excited charm mesons or B decays to two charm mesons, one of which decays semileptonically; candidates where the muon is a misidentified particle, either a pion or a kaon; and combinatorial backgrounds from combinations of unrelated particles from different decay chains.

Since the measurements of the ground states are often affected by the decays of excited states (feed-down), they are usually performed by either measuring only the excited state or by performing a simultaneous measurement of the excited and ground states. Since these different states contain different spin structures, simultaneous measurements allow putting more stringent constraints on models of physics beyond the SM; see Ref. [2].

3.2. Semileptonic Measurements at B Factories

At B factories, B mesons are produced through the decay of $\Upsilon(4S)$. $\Upsilon(4S)$ is the lightest $b\bar{b}$ resonance with mass above the $B\bar{B}$ pair production threshold. This resonance decays almost exclusively in $B^0\bar{B}^0$ and B^+B^- with about the same rate. Due to the small mass difference between the $\Upsilon(4S)$ state and $B\bar{B}$ pairs, the B mesons are generated with very low momentum in the $\Upsilon(4S)$ center of mass. Specifically, the momentum of the B meson is approximately $|\vec{p}_B| \simeq 330\,\text{MeV}$. This is why the decay products of the two Bs are almost isotropically produced in the $\Upsilon(4S)$ rest frame.

At the energy corresponding to the mass of the $\Upsilon(4S)$, the cross-section of the $e^+e^- \to \Upsilon(4S)$ process is approximately 1.06 nb, resulting in about $1.1 \times 10^6/\text{fb}^{-1}$ $B\bar{B}$ pairs. However, at this energy, only about one-fourth of all the hadronic events produced are $\Upsilon(4S)$, with the remainder being non-$B\bar{B}$ events. These events are a background, usually called continuum background. In general, they are rejected exploiting the difference between the topology of particles coming from $\Upsilon(4S)$ decays and from $e^+e^- \to q\bar{q}$ processes: tracks from $e^+e^- \to q\bar{q}$ processes are produced in two opposite jets, while they are spherical for B meson decays.

Semileptonic analyses often benefit from a technique known as B-tagging, which requires reconstructing the signal B meson along with the second B meson present in the event. B-tagging is highly effective in reducing the impact of the continuum background and generally improving event reconstruction.

B-Tagging

In the $\Upsilon(4S) \to B\bar{B}$ decay, there are only two B mesons in the final state. By reconstructing one of them in exclusive decay modes, the rest of tracks and neutrals must come from the other B meson. This technique, called B-tagging, allows considerable reduction in combinatorial and other backgrounds. The tagging B meson is labeled B_{tag} in the following. In addition to background reduction, the information on the direction of B_{tag} is often used to constrain the kinematics of the full event and improve the resolutions in the study of the signal B meson (B_{sig}) decay. B-tagging techniques can be classified in two main approaches:

1. hadronic tagging : the B_{tag} is fully reconstructed into a combination of many different hadronic decay modes. Each decay mode starts from a set of well-reconstructed charm mesons, like D^0, D^+, D^{*+}, D^{*0}, D_s, D_s^* or J/ψ, combined with additional charmless mesons ($\pi^\pm$, $K^\pm$, π^0 and K_s) to form possible B candidates. To optimise efficiency, over a thousand possible decay chains are taken into consideration. The two variables used to test the compatibility with a B meson are:
   (a) $\Delta E = E_B^* - E_{beam}^*$, the difference between the energy of the B candidate in $\Upsilon(4S)$ and the expected B candidate energy fixed by the energy of the beams;

(b) the energy substituted mass, $m_{ES} = \sqrt{E^{*2}_{beam} - |\vec{p}^{\,*}_B|^2}$, where $\vec{p}^{\,*}_B$ is the momentum of the B candidate.

Over time, hadronic B-tagging has been improved by both BABAR and Belle via including more decay modes and using neural networks [35].
The tagging efficiency depends on the multiplicity and the kind of particles present in the analyzed final state. The average overall efficiency is about 0.5% for the tagging B^+ and about 0.3% for B^0 with a purity, which is the probability that a specific decay chain is correctly reconstructed, of about 10–30%. The reconstruction of the four-momentum of the B_{tag} allows determination, event by event, of the four-momentum of the signal B meson (B_{sig}) even in the presence of neutrinos using

$$p_{B_{sig}} = p_{\Upsilon(4S)} - p_{B_{tag}}, \tag{9}$$

where $p_Y(4S)$ is the four-momentum of the initial $\Upsilon(4S)$ which is determined by the energy of the initial electron and positron beams.

2. semileptonic tagging: B_{tag} is reconstructed using $B \to D^* \ell \nu_\ell$ and $B \to D \ell \nu_\ell$ decays. These decays have the highest branching fractions of B decays and comprise more than 7% of B decays. Moreover, the efficiency of reconstructing semileptonic decays is higher than the one of reconstructing fully hadronic B decays. It can range between 0.5 and 1.0% according to the required purity. The downside is that the background is higher than for the hadronic tagging and that the presence of the neutrino on the tag side does not allow for tight kinematic constraints. The key variable to select the tag side is the cosine of the angle between the B candidate and the visible system Y,

$$\cos\theta_{BY} \equiv \frac{2E_B E_Y - m_B^2 - m_Y^2}{2|p_B||p_Y|}, \tag{10}$$

where $Y \equiv D\ell$ or $D^*\ell$. The energies and momenta of the B meson and the Y system are computed in the $\Upsilon(4S)$ rest frame, and these are well known from the parameters of the accelerator. For a single massless particle missing, $cos\theta_{BY}$ is limited to the physical range of -1 to 1. Instead, for an incorrectly identified tag-side, due to $B \to D^{**}\ell\nu$ or other decays with a $D^{*(*)}$ and a lepton in the final state, it can extend beyond these boundaries due to additional missing particles.

3.3. Experiments at LHC

The production mechanism of b quarks at hadron colliders are quark annihilation $q\bar{q} \to b\bar{b}$ and gluon fusion processes $q\bar{q}, gg \to b\bar{b}$, where the latter ones are dominating [36]. These different processes have different final state kinematics. The gluon splitting produces $b\bar{b}$ pairs with a small opening angle and small transverse momentum, p_T. In the forward (and backward) direction, gluon splitting is the dominant process, which is what the LHCb detector is designed for [37]. Since all b-hadron species are created, such as B^+, B^0, B^0_s, B^+_c, and Λ^0_b, the range of possible LFU measurements can be greatly expanded compared to the measurements from the B factories.

The LHCb experiment covers the forward acceptance with pseudorapidity η in the range of $2 < \eta < 5$. This corresponds only to 4% of the full solid angle, but captures about 25% of the total $pp \to b\bar{b}$ event cross-section. In the pseudorapidity range of $2 < \eta < 5$, the visible b-hadron cross section was measured to be 72 μb at 7 TeV and almost double at 13 TeV with about 144 μb [38]. Details about the various subdetectors and the overall performances are described in Ref. [37,39].

The acceptance of the general purpose experiments CMS and ATLAS is limited to the central region of $|\eta| < 2.2$. This makes the experiments 40% efficient for $pp \to b\bar{b}$ processes. For the time being, the only semileptonic $b \to c$ measurement performed is a measurement of $B_c \to J/\psi\tau\nu$ decays by CMS [40]. This result is summarized in Section 4.2.3.

The LHCb experiment recorded 3 fb^{-1} of data in 2011–2012 at $\sqrt{s}$ = 7–8 TeV (Run 1) and 6 fb^{-1} in 2015–2018 at $\sqrt{s}$ = 13 TeV (Run 2). In 2018, the CMS experiment recorded 59.7 fb^{-1} of pp data at $\sqrt{s}$ = 13 TeV, which is analyzed for the measurement of ratio $\mathcal{R}(J/\psi)$. During Run 3, which started in 2022, both LHCb and CMS were recording data at $\sqrt{s}$ = 13.6 TeV. So far, no LFU measurements have been published using this dataset.

The advantage of a large amount of b quarks comes at the price of large amounts of background. The LHC experiments cannot rely on the full reconstruction of the rest of the event; hence, other reconstruction techniques are used to suppress various backgrounds which are explained in the following sections.

3.4. Semileptonic Measurements at LHCb

At LHCb, the momentum of the b hadrons in production is not known, so the identification of semileptonic events relies almost exclusively on the very good vertex reconstruction capabilities for the identification of the B flight direction and the secondary decay vertices. LHCb has an excellent muon reconstruction. Electrons, however, are affected by bremsstrahlung that degrades their momentum reconstruction. Therefore, most LFU measurements in LHCb consider only muons. Recent improvements on the electron reconstruction have encouraged ongoing analyses with electrons.

The b hadrons produced in LHCb are highly boosted ($\beta\gamma \approx 50$) in the forward direction such that they have a mean flight length of about 1 cm. Together with the high resolution on the vertex position, this is crucial for the reconstruction of the signal event. The separation between the B decay vertex and the primary vertex, PV, mainly reduces the combinatorial background. In addition, since the decay products of the second b hadron, which usually is produced within LHCb's acceptance, are well separated in η, the wrong assignment of tracks from the other b hadron is negligible.

Over 99% of inelastic pp collisions do not produce b quarks, making them a significant source of background. Therefore, the trigger must be efficient in detecting b hadrons while having a high rejection rate for backgrounds. In LHCb, the trigger takes advantage of the long lifetime of b hadrons. As these particles have a relatively large mass, their decay products have an average p_T higher than typical particles produced in pp collisions. The trigger uses a combination of hardware (L0) and software stages. The L0 trigger relies primarily on the muon detector and the calorimeter response and is very efficient in triggering muons. However, since muons from tau decays have a much lower (transverse) momentum than muons that come directly from the B meson decay, muon triggers are inefficient for selecting the signal channels for measurement of LFU ratios and therefore not used. Instead, the hadrons in the decay are used to trigger on, which are the same for the signal and normalization channel.

At the luminosity of the Large Hadron Collider (LHC), a significant number of multiple proton–proton collisions occur simultaneously in the same bunch crossing. To improve measurements with b hadrons, which need well-reconstructed production and decay vertices, LHCb reduces the luminosity locally to 1.8 visible collisions per bunch crossing on average during Run 1 and Run 2.

Reconstructing B Kinematics

All muonic analyses use kinematic variables that are selected to offer a good discrimination between signal and normalization channels, as well as other backgrounds. To use these, one needs to proceed to the B candidate rest frame. Since the B momentum cannot be fully reconstructed in hadron colliders, an approximation must be made. Different approximations are used by the LHCb and CMS experiments. The analyses performed by LHCb assume that the boost of the visible B decay products along the beam axis is equal to that of the b hadron: $(\gamma\beta_z)_B \approx (\gamma\beta_z)_{B_{\text{vis}}}$. CMS instead uses the assumption that the four-momentum of the B equals the four-momentum of its visible decay products, scaled by the mass of the B according to the PDG: $p_B = m_B/m_{\text{vis}} \cdot p_{\text{vis}}$.

Then, kinematic variables can be defined: the muon energy in the B rest frame, E_μ^*; the missing mass squared, $m^2_{\text{miss}} = (p_B - p_D - p_\mu)^2$; and the squared four-momentum transfer to the lepton system, $q^2 = (p_B - p_D)^2$. The muon energy is much higher for the normalization channel than for muons coming from tau decays, where a significant amount of energy is attributed to the neutrinos in the tau decay. The missing mass squared variable represents the invariant mass of the neutrinos and thus peaks around zero for muon decays, while it has higher values for the tauonic decay. The energy transferred by the lepton pair, q^2, is higher for tau decays than for the normalization channels.

Backgrounds from partially reconstructed B decays, including backgrounds with two charmed hadrons, can be suppressed by using isolation requirements. This ensures there are no other charged or neutral particles around the signal candidate and naturally suppresses partially reconstructed decays. A common method used in the LHCb measurements, described in Ref. [41], uses a multivariate analysis (MVA) method. Based on the track's separation from the PV and decay vertex, the angle between the track and candidate momentum vector, and the decay length significance under the hypothesis that the track does or does not originate from the candidate, the algorithm assigns a value on the likelihood of the track originating from the signal B candidate or from the rest of the event. A cut on this value reduces the number of partially reconstructed background events.

3.5. Tau Decays

Measurements of LFU in semileptonic $b \to c$ decays can be split by the τ decay mode, which can be leptonic or hadronic. Each comes with its own advantages and disadvantages. The leptonic τ decays are either $\tau^- \to \mu^- \overline{\nu}_\mu \nu_\tau$ or $\tau^- \to e^- \overline{\nu}_e \nu_\tau$ decays, which thus introduce an additional two neutrinos in the final state. The benefit of these decay channels is that the final states of both the signal and normalization channels are equal, which results in a cancellation of many systematic uncertainties related to the light lepton. It also allows extraction of $\mathcal{R}(H_c)$ from a single dataset.

Hadronic decays can be split according to the number of charged pions into one-prong, $\tau^- \to \pi^-(\pi^0)\nu$, and three-prong, $\tau^- \to \pi^-\pi^+\pi^-(\pi^0)\nu$, decays. The three-prong decays offer a possibility to reconstruct the τ decay vertex and hence suppress backgrounds by requiring a distance between the B and the τ vertex. This works only for the LHCb experiment, since the B decays at B factories are not produced with enough boost to sufficiently displace the τ vertex. The one-prong decays, one the other hand, are only used at B factories. At the LHC, these decays are too difficult to reconstruct and distinguish from backgrounds. Both of these decays result in different signals and normalization modes in LFU ratios. Therefore, they are measured with respect to another hadronic decay, and ratio $\mathcal{R}(H_c)$ is calculated using external inputs. More precise determinations of those inputs results in more precise measurements of $\mathcal{R}(H_c)$.

4. Tests of Lepton Universality

In this section, we describe the most recent measurement of semitauonic results performed at the B factories and at the LHC.

4.1. Measurements of $\mathcal{R}(D)$ and $\mathcal{R}(D^*)$

4.1.1. B Factory Measurements with Muonic τ Decays

The first precise measurement of $\mathcal{R}(D^{(*)})$ was performed by BABAR using the full dataset of 471×10^6 $B\bar{B}$ pairs [42,43]. The Belle experiment followed with an analysis of their 772×10^6 $B\bar{B}$ pairs using a similar analysis strategy [44].

Both analyses use the hadronic B-tagging approach. The signal and the normalization channels are selected using the same particles in the final state. The event selection requires the reconstruction of a D or D^* meson and a charged lepton ℓ that can be an electron or a muon ($\ell = e$ or μ). The events are required to have a well-reconstructed B_{tag} and no additional tracks. The D^0 and D^+ mesons are reconstructed using different combinations

of K^+, K^0_s, and $\pi^{0,+}$ with an invariant mass close to the nominal D meson masses. The higher-mass D^{*0} and D^{*+} mesons are identified by their $D^* \to D\pi$ and $D^* \to D\gamma$ decays.

The reconstruction of the B_{tag} strongly reduces the non-$B\bar{B}$ background and misreconstructed events. The remaining backgrounds are further reduced by using outputs from multivariate classifiers. A key variable used in the multivariate classifier is the sum of the energy deposits in the calorimeter that is not associated with the signal or the B_{tag} (usually called E_{ECL} or E_{extra}). This quantity is used as input to the multivariate classifiers designed to reject events with additional neutral clusters, like D^{**} meson decays with π^0 mesons in the final state. The multivariate classifiers are trained using MC samples.

The BABAR measurement requires a minimum value for the output of the classifier to select signal-enriched events. The signal determination employs a two-dimensional fit to the square of the invariant mass of the undetected particles, defined as $m^2_{miss} = p^2_{miss} = (p_{B_{sig}} - p_{D^{(*)}} - p_\ell)^2$ (where $p_{B_{sig}}$, $p_{D^{(*)}}$ and p_ℓ denote the four-momenta of B_{sig}, the $D^{(*)}$ meson, and the charged lepton, respectively) and the magnitude of the lepton momentum in the B_{sig} rest frame ($|p^*_\ell|$). Belle instead performed a simultaneous one-dimensional fit to the m^2_{miss} in the $m^2_{miss} < 0.85$ GeV^2 region, which is dominated by the normalization decays, and a one-dimensional fit to the output of the multivariate classifier (O'_{NB}) in the high m^2_{miss} region, which is a region enriched by the signal. The shape of the probability distribution functions that describe each of the contributions is taken from MC simulations, with various assumptions on the signal and normalization form factors and on the composition for the various backgrounds. Both experiments determine the yields for the signal and normalization B decays and background contributions using a maximum likelihood fit for the $D^0\ell$, $D^+\ell$,$D^{*0}\ell$, and $D^{*+}\ell$ data samples. The final results are obtained assuming isospin relations between the various modes, adding constraints based on the known branching fractions and simulated relative efficiencies. In Figure 2, selected projections for the BABAR fit result are shown for illustration.

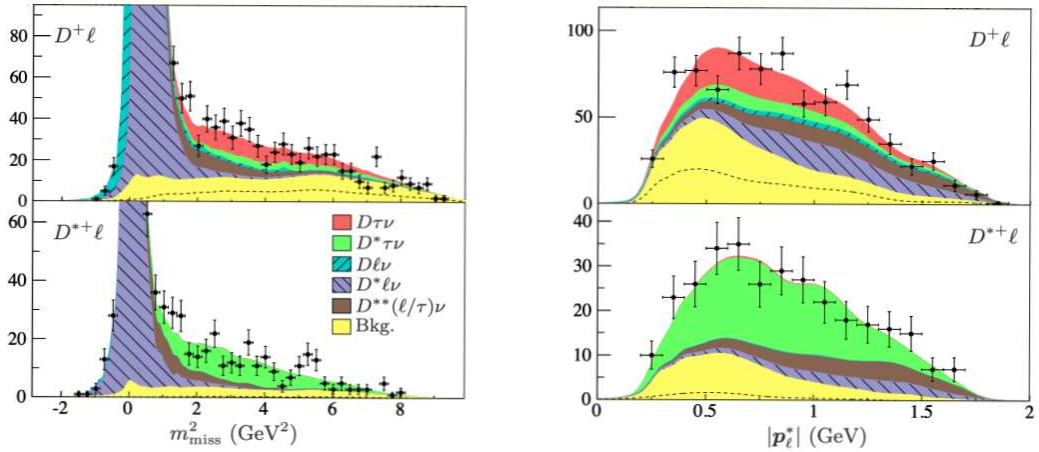

Figure 2. Distributions of the square of the missing mass, m^2_{miss} (**left**), and the magnitude of the momentum of the charged lepton in the B_{sig} rest frame, $|p^*_\ell|$, (**right**) for $B^0 \to D^+\ell\nu$ (**top**) and $B^0 \to D^{*+}\ell\nu$ (**bottom**) candidates as obtained by the BABAR measurement [42,43]. The distributions of $|p^*_\ell|$ shown here are obtained in the signal enriched region $m^2_{miss} > 1\,\text{GeV}^2$.

Semileptonic B decays to higher-mass D^{**} mesons are, among the various background contributions, the most challenging because their branching fractions and form factors are not well known. Since the D^{**} mesons decay to a D or a D^* meson plus additional particles, the $\bar{B} \to D^{**}\ell\nu_\ell$ components have a broader m^2_{miss} distribution that can mimic the signal. These contributions are estimated by special control samples based on the same signal selection but requiring an additional reconstructed π^0 meson. These special control samples have values of m^2_{miss} close to zero for decays of the form $\bar{B} \to D^{(*)}\pi^0\ell\nu_\ell$. The fit to these samples is performed simultaneously with the fit to the signal. It is worth noticing

that both BABAR and Belle restrict the data to $q^2 > 4$ GeV^2 to enhance the contribution from signal decays. The low-q^2 region is used as an additional sample to control shapes and efficiencies of the normalization components.

The ratio of branching fractions is calculated as

$$\mathcal{R}(D^{(*)}) = \frac{N_{sig}}{N_{norm}} \frac{\epsilon_{norm}}{\epsilon_{sig}}, \tag{11}$$

where N_{sig} and N_{norm} are the number of signal and normalization events determined by the fit and $\epsilon_{norm}/\epsilon_{sig}$ is the ratio of efficiencies which is determined from simulation. Signal efficiency ϵ_{sig} includes the branching ratio of $\tau \to \ell\nu_\ell\nu_\tau$ decays which is about 17.4% for both the electron and muon decay modes.

Most of the systematic uncertainties cancel in these measurements because the signal and the normalization decay are reconstructed with the same particles in the final state. For both BABAR and Belle, the largest systematic uncertainties come from the limited size of the simulation samples and the contribution from $\overline{B} \to D^{**}\ell\nu_\ell$ decays.

BABAR finds the following results:

$$\begin{aligned} \mathcal{R}(D) &= 0.440 \pm 0.053\,(\text{stat}) \pm 0.042\,(\text{syst}), \\ \mathcal{R}(D^*) &= 0.332 \pm 0.024\,(\text{stat}) \pm 0.018\,(\text{syst}), \end{aligned}$$

with a correlation of $\rho = -0.27$, and Belle finds

$$\begin{aligned} \mathcal{R}(D) &= 0.375 \pm 0.064\,(\text{stat}) \pm 0.026\,(\text{syst}), \\ \mathcal{R}(D^*) &= 0.293 \pm 0.038\,(\text{stat}) \pm 0.015\,(\text{syst}), \end{aligned}$$

with a correlation of $\rho = -0.49$. The two results are compatible within the uncertainties. The statistical uncertainty dominates the total uncertainties. BABAR also performs fits without assuming isospin constraints, and the results are consistent with the expected small degree of isospin breaking.

The Belle II collaboration recently released the first measurement of $\mathcal{R}(D^*)$ [45] using a data sample corresponding to 198×10^6 $B\bar{B}$ pairs collected in the 2019–2021 data-taking period. The tag-side reconstructed algorithm used is an improved version of the Belle hadronic B-tagging. This new algorithm is known as Full Event Interpretation (FEI) [46]. It performs a hierarchical reconstruction of the B-meson decay chains using a multivariate classification at each stage. The algorithm starts from final state particles (leptons, pions, kaons, and photons) and employs reconstructions of various intermediate possible particles (D, D^*, K^0_s, J/ψ and π^0 mesons) which can belong to the B meson decays. The algorithm reconstructs about 10^4 unique B meson decay chains. From each unique decay chain, a BDT is trained to classify whether or not the particles are correctly reconstructed. The final classifier provides the FEI probability for the tagging B meson to be correctly reconstructed. The B_{tag} reconstructed with FEI is required to have a beam energy difference $\Delta E = E_{tag} - E_{beam}$ close to zero and $m_{ES} > 5.27\,\text{GeV}$. Finally, for each event, only the candidate with the highest FEI probability is kept. Compared with the Belle hadronic B-tagging, the FEI has a 2–3 times higher efficiency.

The signal B-meson candidate is reconstructed by combining a D^* meson and a lepton. The D^* mesons are reconstructed in $D^0\pi^+$, $D^+\pi^0$ and $D^0\pi^0$ decay modes. The D^+ and the D^0 are reconstructed in various decay modes to increase signal efficiency. Also in this analysis, the signal region is defined by requiring $q^2 > 4.0\,\text{GeV}^2$.

Ratio $\mathcal{R}(D^*)$ is extracted from an extended two-dimensional likelihood fit to the binned m^2_{miss} and E_{ECL} distributions using Equation (11). The three different D^* modes are fit simultaneously assuming isospin asymmetry for charged and neutral B meson decays setting $\mathcal{R}(D^{*0}) = \mathcal{R}(D^{*+})$. The final result is

$$\mathcal{R}(D^*) = 0.262^{+0.041}_{-0.039}\,(\text{stat})^{+0.035}_{-0.032}\,(\text{syst}),$$

where the systematic uncertainty is dominated by the knowledge of the shapes of the PDFs and the limited simulated sample.

4.1.2. Semileptonic Tagging

The Belle collaboration also used the semileptonic tagging technique to study semi-tauonic decays. The first measurement of $\mathcal{R}(D^*)$ based on this tagging approach was released in 2016 [47]. This was superseded by the measurement of the combined $\mathcal{R}(D)$ and $\mathcal{R}(D^*)$ [48]. This measurement uses the FEI algorithm applied to identify the B_{tag} but reconstructed through its semileptonic $B \to D^{(*)}\ell\nu$ decays. The signal side is reconstructed by combining D and D^* mesons with lepton candidates. The analysis uses D^0 and D^+ mesons, reconstructed in many different decay modes, to increase signal efficiency. The D^* mesons are reconstructed using both charged and neutral slow pions and photons. In events with multiple candidates, only the combination with the highest FEI probability is retained. The signal and the normalization channels are separated using a BDT exploiting various event features. The most discriminating ones are the $\cos\theta_{BY}$ for the signal side, the missing mass squared, m^2_{miss}, and the total energy of all reconstructed particles in the event. The output of the BDT is used, together with the E_{ECL}, to disentangle the signal, normalization, and remaining background contributions. The final fit assumes isospin symmetry, fixing $\mathcal{R}(D^0) = \mathcal{R}(D^+)$ and $\mathcal{R}(D^{*+}) = \mathcal{R}(D^{*0})$. The fit projections are shown in Figure 3 (bottom), and the results are

$$\begin{aligned} \mathcal{R}(D) &= 0.307 \pm 0.037\,(\text{stat}) \pm 0.016\,(\text{syst}), \\ \mathcal{R}(D^*) &= 0.283 \pm 0.018\,(\text{stat}) \pm 0.014\,(\text{syst}), \end{aligned}$$

with a total correlation of $\rho = -0.52$ between the two values. Also in this analysis, the largest source of systematic is the limited size of the simulated sample, which is used to make the templates used in the fit and also to train the multivariate selection.

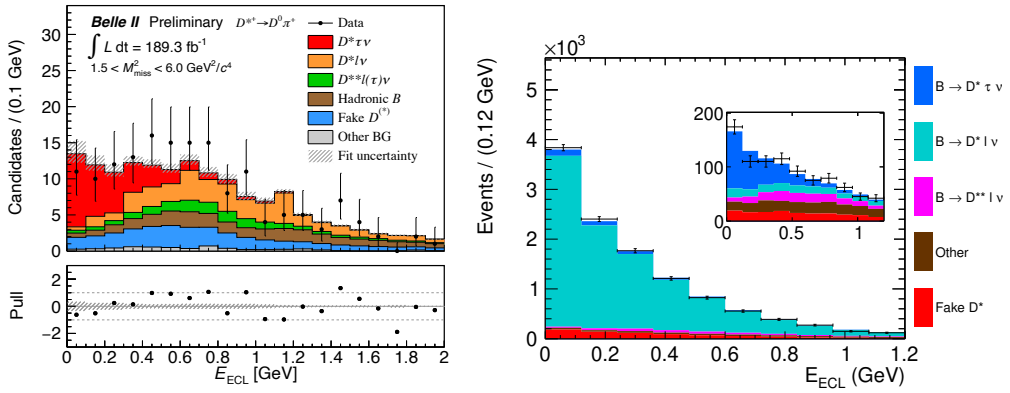

Figure 3. (**Left**): the distribution of E_{ECL} as obtained by the Belle II measurement [45] in the region of $1.5 < m^2_{miss} < 6.0\,\text{GeV}^2$ for the $D^{*+} \to D^0\pi^+$ candidates. (**Right**): distribution of E_{ECL} with the fit results from Belle measurement superimposed [48]. The data shown are for $D^{*+}\ell$ combinations. The inset shows the same distribution in the signal enriched region defined by a tight requirement on the output of the BDT classifier.

4.1.3. Belle Measurement with Hadronic τ Decays

The Belle experiment measured $\mathcal{R}(D^*)$ with hadronic $\tau \to \pi\nu$ and $\tau \to \rho\nu$ decay modes [49,50]. The measurement provides primarily the first measurement of the τ polarization fraction $P_\tau(D^*)$.

The analysis strategy is similar to that of the hadronic tag described in Section 4.1.1. The background is reduced, retaining only events with $q^2 > 4\,\mathrm{GeV}^2$ and with $|\cos\theta_h| < 1.0$, where $\cos\theta_h$ is the helicity angle of the π or ρ mesons from the τ decay. The signal yield is normalized to $B \to D^*\ell\nu$ events, which are identified using only m^2_{miss}. Angle θ_h is reconstructed by taking advantage of the fully reconstructed B_{tag} to boost the visible τ daughters into the $\tau\nu$ lepton pair system, whose four-momentum is given by $p_{\tau\nu} = p_{B_{sig}} - p_{D^*}$. Observables $\mathcal{R}(D^*)$ and $P_\tau(D^*)$ are extracted fitting E_{ECL} in two bins of θ_h, simultaneously for $\tau \to \pi\nu$ and $\tau \to \rho\nu$. The results are

$$\begin{aligned} \mathcal{R}(D^*) &= 0.270 \pm 0.035\,(\mathrm{stat})^{+0.028}_{-0.025}\,(\mathrm{syst}), \\ P_\tau(D^*) &= -0.38 \pm 0.51\,(\mathrm{stat})^{+0.028}_{-0.016}\,(\mathrm{syst}), \end{aligned}$$

with a total correlation of $\rho = 0.33$. These results are in agreement with the SM expectations shown in Tables 1 and 2.

4.1.4. Measurement of $\mathcal{R}(X_{\tau/\ell})$

The Belle II collaboration presented the first measurement [51] of the ratio $\mathcal{R}(X_{\tau/\ell})$ of the branching fractions of inclusive B-meson decays $\mathcal{R}(X_{\tau/\ell}) = \mathcal{B}(\bar{B} \to X\tau\nu_\tau)/\mathcal{B}(\bar{B} \to X\ell\nu_\ell)$, where $\ell = e$ or μ. The measurement is based on a sample of about 198×10^6 $B\bar{B}$ pairs. This analysis uses the hadronic B-tagging to fully reconstruct the B_{tag} and groups the rest of the particles, which must include a lepton, with the signal side B_{sig}. The lepton is a well-identified electron or muon. If the lepton comes from the τ lepton decay in process $\bar{B} \to X\tau\nu_\tau$, the event is considered to be signal; if the lepton comes from decay $\bar{B} \to X\ell\nu_\ell$, it is considered normalization.

The signal and the normalization yields are extracted with a two-dimensional fit to the lepton momentum in the B_{sig} rest frame, p^*_ℓ, and the $m^2_{miss} = (P_{sig} - P_X - P_\ell)$, where P_X is the four-momentum of hadronic system X. All tracks and energy clusters in the calorimeter, which are not associated with the B_{tag} or the lepton, are used to reconstruct hadronic system X. Particular care has to be taken to select good-quality tracks consistent with originating from the interaction point. The clusters are also required to release a minimum energy in the electromagnetic calorimeter. The mass of hadronic system M_X is the invariant mass of all reconstructed particles associated with the X system.

The fit results are shown in Figure 4. The resulting value for $\mathcal{R}(X_{\tau/\ell})$, averaging the muon and electron samples, is

$$\mathcal{R}(X_{\tau/\ell}) = 0.228 \pm 0.016\,(\mathrm{stat}) \pm 0.036\,(\mathrm{syst}), \tag{12}$$

which is in agreement with the SM prediction from Ref. [52]. The largest systematic uncertainties are due to the limited size of the simulation sample, the discrepancy between the inclusive semileptonic branching fraction and the sum of the known exclusive semileptonic decays, and the form factors of the various exclusive decays entering the model of the X system.

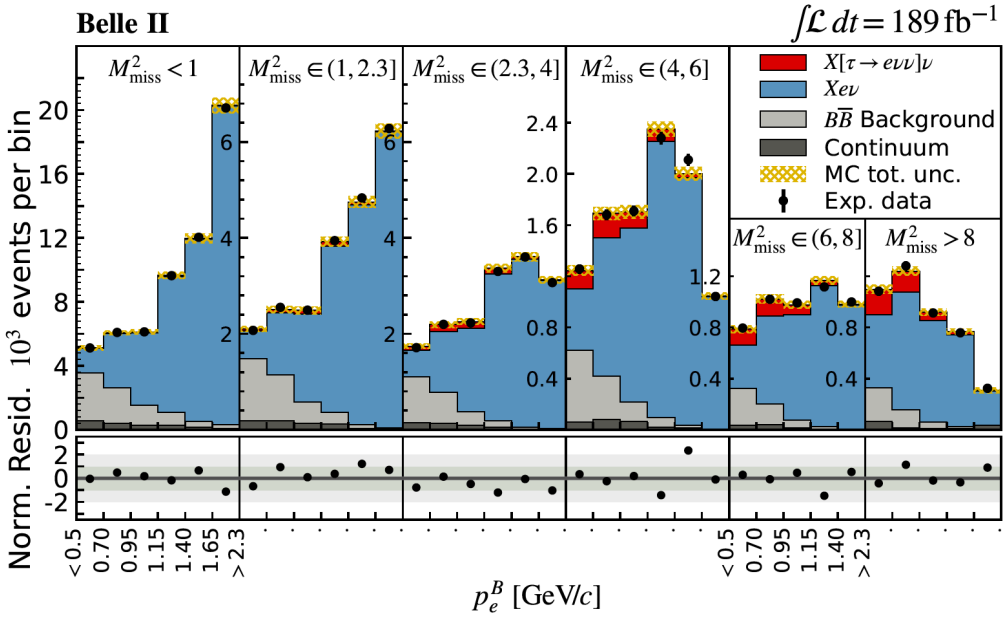

Figure 4. Distribution of the electron momentum p_e^* in bins of m^2_{miss} from the inclusive measurement of $\mathcal{R}(X_{\tau/\ell})$ by Belle II [51]. As expected, signal $B \to X\tau\nu$ is visible in the bins with a high value of m^2_{miss} and a low value of p^*_ℓ.

4.1.5. LHCb Measurements with Muonic τ Decays

The first measurement of LFU in semileptonic $b \to c$ decays from the LHCb experiment was a measurement of ratio $\mathcal{R}(D^*) = \mathcal{B}(\overline{B}^0 \to D^{*+}\tau^-\overline{\nu}_\tau)/\mathcal{B}(\overline{B}^0 \to D^{*+}\mu^-\overline{\nu}_\mu)$, which looked at $\tau^- \to \mu^-\overline{\nu}_\mu\nu_\tau$ decays [41] and was superseded by the combined measurement of $\mathcal{R}(D^0)$ and $\mathcal{R}(D^*)$, where the D^* refers to both D^{*+} and D^{*0} [53]. This analysis reconstructs $D^0 \to K^-\pi^+$ decays combined with muons using LHCb's Run 1 data set. This sample is split into two mutually exclusive datasets, referred to as the $D^0\mu^-$ and $D^{*+}\mu^-$ samples. If a D^0 candidate combined with any track in the event forms a D^{*+} candidate, then this is part of the $D^{*+}\mu^-$ sample. This sample contains $\overline{B}^0 \to D^{*+}\ell^-\overline{\nu}_\ell$ decays. The other events are form the $D^0\mu^-$ sample, which contains $B^- \to D^0\ell^-\overline{\nu}_\ell$, as well as partially reconstructed $B^- \to D^{*0}\ell^-\overline{\nu}_\ell$ and $\overline{B}^0 \to D^{*+}\ell^-\overline{\nu}_\ell$ decays. In the subsequent $D^{*0} \to D^0\gamma$ and $D^{*0} \to D^0\pi^0$ decays, the photons and neutral pions are not reconstructed. Analyzing these two samples simultaneously helps constrain common fit parameters.

The templates to model the signal and normalization channels as well as those to describe partially reconstructed backgrounds are based on simulated samples. Two independent fit model implementations, using different corrections for form factors and simulation, are used to cross-check most aspects of the analysis. The form factors are weighted using the latest parameterizations; see [53]. Also, the form factors for the backgrounds from the excited D^{**} states are updated with respect to the first measurement.

To constrain the background contributions, six distinct control regions are defined with enhanced levels of background contributions. They are enhanced in B to two charm mesons by requiring an extra charged kaon around the signal candidate; in B to D^{**} mesons by requiring an extra pion; and in decays to heavy D^{**} mesons by requiring an extra pair of pions with opposite charge. These three types of control regions are defined for both the $D^{*+}\mu^-$ and $D^0\mu^-$ samples, creating a total of eight regions which are fit simultaneously.

The decay modes are measured using a three-dimensional template fit using m^2_{miss}, E^*_μ and q^2 variables. The fit results for both samples are shown for the highest q^2 bin in

Figure 5. After correcting for the efficiencies of reconstructing the signal and normalization mode, they yield a value of

$$\begin{aligned}\mathcal{R}(D^{*+}) &= 0.281 \pm 0.018\,(\text{stat}) \pm 0.024\,(\text{syst}),\\ \mathcal{R}(D^{0}) &= 0.441 \pm 0.060\,(\text{stat}) \pm 0.066\,(\text{syst}),\end{aligned}$$

with a correlation of $\rho = -0.43$, which is about 2σ above the SM predictions.

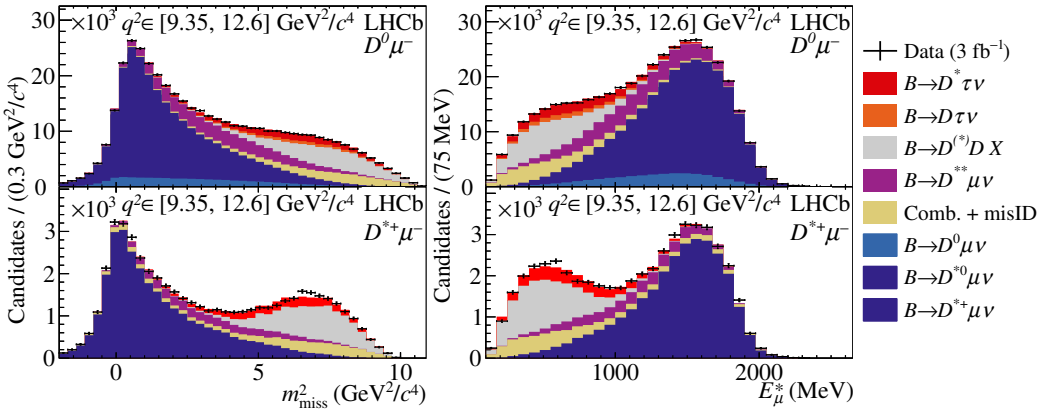

Figure 5. Distributions of (**left**) m^2_{miss} and (**right**) E^*_μ in the highest q^2 bin (above 9.35 GeV$^2/c^4$) of the (**top**) $D^0\mu^-$ and (**bottom**) $D^{*+}\mu^-$ signal data of LHCb's $\mathcal{R}(D^{(*)})$ measurement [53], overlaid with projections of the fit model.

The measurement of $\mathcal{R}(D^+)$ and $\mathcal{R}(D^{*+})$ looks at $D^{*+} \to D^+\pi^0$ decays, where the π^0 is not reconstructed and largely follows the strategy of LHCb's $\mathcal{R}(D^{(*)})$ measurement [54]. It analyzes part of LHCb's Run 2 data set: the 1.9 fb^{-1} recorded in 2015 and 2016. The main objective of the measurement is $\mathcal{R}(D^+)$; hence, the selection strategy is optimized for this decay. Through feed-down from D^{*+} decays, the measurement also has access to $\mathcal{R}(D^{*+})$.

To reduce the large CPU resources needed for large MC samples, the MC only simulated tracking detectors (Tracker-Only), and new methods are developed to emulate the trigger selection. Another newly developed method is the use of the HAMMER tool [30,55] to weight MC samples to different form factor parameterizations.

Four data sets are defined based on the response to the track-isolation algorithm: the signal region, samples with one or two extra charged pions to constrain backgrounds with D^{**} decays, and a sample with an additional charged kaon to control backgrounds from B mesons to two charm hadrons. Shape variations in these backgrounds are constrained from the non-signal region samples, except for backgrounds of $\Lambda_b^0 \to D^+ n\mu^-\overline{\nu}_\mu$. These are allowed to have a different shape in the signal region because the neutron does not show up in the control regions with charged tracks.

The four regions are fitted simultaneously in a three-dimensional template fit in bins of q^2, E^*_μ, and m^2_{miss} and the following values are found for $\mathcal{R}(D^+)$ and $\mathcal{R}(D^{*+})$:

$$\begin{aligned}\mathcal{R}(D^{+}) &= 0.249 \pm 0.043\,(\text{stat}) \pm 0.047\,(\text{syst}),\\ \mathcal{R}(D^{*+}) &= 0.402 \pm 0.081\,(\text{stat}) \pm 0.085\,(\text{syst}),\end{aligned}$$

with a correlation of $\rho = -0.39$. The result is consistent with the SM. The dominating systematic uncertainties are due to the limited sample size of the simulated data, the template shape from double-charm backgrounds, and the uncertainties on the form factor parameters.

4.1.6. LHCb Measurements with Hadronic τ Decays

Analyses with hadronic τ decays in LHCb use the three-prong τ decays and exploit the separation between the H_c and the τ vertex to suppress backgrounds. For hadronic τ

decays, the most abundant types of backgrounds by far are double-charm backgrounds, $H_b \to H_c D(X)$, where D can be a D_s^+, D^+, or D^0 meson which decays to three charged pions. The most dominant one is the background with D_s^+ mesons, which has been studied in great detail in Ref. [56] and before in Ref. [57]. The three-prong τ decay happens predominantly via the $a_1 \to \rho^0 \pi^-$ decay, while the D_s^+ decays mainly through the η and η' resonances. These different resonance structures, together with other decay modes, are exploited by a BDT to separate between signal and background.

Ratio $\mathcal{R}(D^*)$ has been measured twice by LHCb using three-prong τ decays, once with the Run 1 data [57] and once with the first part of the Run 2 data set [56], recorded in 2015 and 2016. The analyses use the normalization channel $\bar{B}^0 \to D^{*+}\pi^-\pi^+\pi^-$ to determine ratio

$$\mathcal{K}(D^*) = \frac{\mathcal{B}(\bar{B}^0 \to D^{*+}\tau^-\bar{\nu}_\tau)}{\mathcal{B}(\bar{B}^0 \to D^{*+}\pi^-\pi^+\pi^-)}, \tag{13}$$

from which ratio $\mathcal{R}(D^*)$ can be determined with external input.

For the signal channel, a fit is performed with three variables: the decay time of the three pions (t_τ), q^2, and the output of the BDT used to suppress backgrounds coming from doubly charmed $H_b \to D^{*-}D_s^+X$ decays. Projections of the fits for each of these variables are shown in Figure 6. The analyses yield the following values for the Run 1 and Run 2 data sets:

$$\begin{aligned} \mathcal{K}(D^*)_{\text{Run1}} &= 1.93 \pm 0.12\,(\text{stat}) \pm 0.17\,(\text{syst})\,, \\ \mathcal{K}(D^*)_{\text{Run2}} &= 1.79 \pm 0.11\,(\text{stat}) \pm 0.11\,(\text{syst})\,. \end{aligned}$$

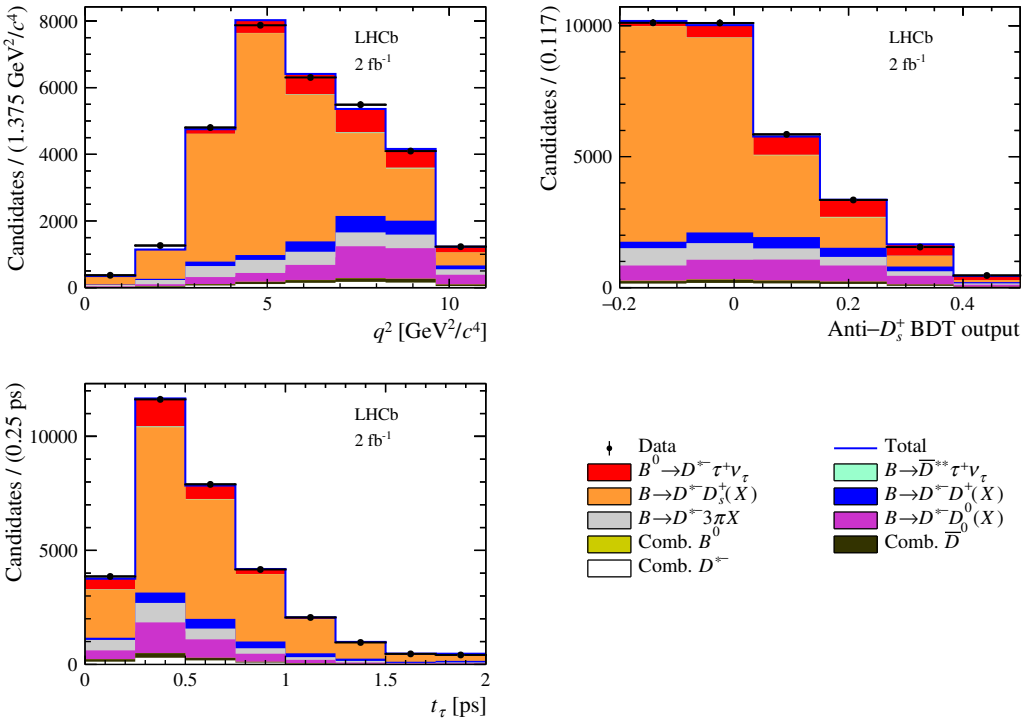

Figure 6. Fit projections of the three-dimensional fit of the **(top left)** q^2, **(top right)** BDT output and **(bottom left)** 3π decay time distributions from LHCb's hadronic $\mathcal{R}(D^*)$ measurement [56].

Using the latest PDG averages of the branching fractions of the control and normalization channels, the value of $\mathcal{R}(D^*)$ can be calculated as

$$\begin{aligned} \mathcal{R}(D^*)_{\text{Run1}} &= 0.291 \pm 0.019\,(\text{stat}) \pm 0.026\,(\text{syst}) \pm 0.013\,(\text{ext})\,, \\ \mathcal{R}(D^*)_{\text{Run2}} &= 0.260 \pm 0.015\,(\text{stat}) \pm 0.016\,(\text{syst}) \pm 0.012\,(\text{ext})\,. \end{aligned}$$

The systematic uncertainties were largely reduced in Run 2 measurement. The largest systematic uncertainty is still the limited size of the simulated data samples, but no longer by far. This is followed by the uncertainties on the signal template shape and the knowledge of the double charm background parameters. When combined, these results yield the following value:

$$\mathcal{R}(D^*) \quad = \quad 0.267 \pm 0.012\,(\text{stat}) \pm 0.015\,(\text{syst}) \pm 0.013\,(\text{ext})\,.$$

This combination, as well as the individual results, is compatible with the SM prediction and is one of the most precise measurements of $\mathcal{R}(D^*)$ to date.

4.2. Measurements of $\mathcal{R}(J/\psi)$ and $\mathcal{R}(\Lambda_c^+)$

Measurements of ratios of other semileptonic $b \to c$ decays can provide constraints to new physics scenarios complementary to those derived from $\mathcal{R}(D)$ measurements. This section discusses the results from measurements with $B_c \to J/\psi\,\ell\nu_\ell$ and $\Lambda_b \to \Lambda_c\ell\nu_\ell$ decays. Since Λ_b and B_c hadrons are not created at the B factories, these measurements are performed only at the LHC.

4.2.1. $\mathcal{R}(\Lambda_c^+)$ at LHCb

The half-integer spin of the Λ_b^0 initial state [31,58] offers complementary constraints to the existing measurements of $\mathcal{R}(D)$. In the SM, the value of $\mathcal{R}(\Lambda_c^+)$ is predicted to be $\mathcal{R}(\Lambda_c^+) = 0.324 \pm 0.004$ [31,32]. This analysis [59] uses LHCb's Run 1 dataset and studies the three-prong τ^- decay. The normalization channel used is the $\Lambda_b^0 \to \Lambda_c^+ 3\pi$ decay such that many systematic uncertainties in the reconstruction of the signal and normalization channel cancel in the ratio.

Similar to the hadronic $\mathcal{R}(D^*)$ analysis, the separation between the Λ_c baryon and three-prong vertex in the signal is exploited by requiring the difference in the positions of these vertices along the direction of the beam to be at least five times larger than its uncertainty. Double-charm backgrounds, in particular those with a D_s meson, are suppressed by the same BDT as in Ref. [57]. The signal yield is extracted in a three-dimensional binned maximum-likelihood fit, in bins of the double-charm BDT output, the τ lifetime, t_τ, and q^2. Results of the fits in the q^2 variable for the low- and high-BDT region are shown in Figure 7. The significance of the signal in the fit is found to be 6.1σ.

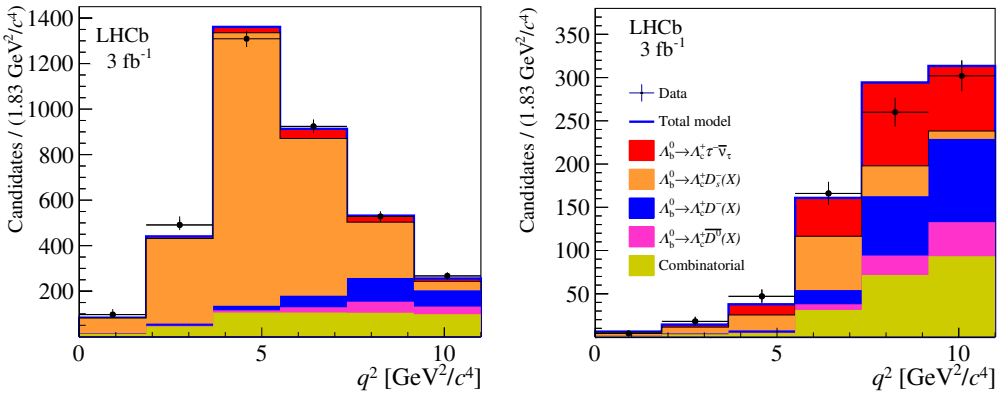

Figure 7. Distributions of q^2 for $\Lambda_b \to \Lambda_c\tau\nu_\tau$ candidates having a BDT output value (**left**) below and (**right**) above 0.66 for LHCb's $\mathcal{R}(\Lambda_c^+)$ measurement [59]. Projections of the three-dimensional fit results are overlaid. The various fit components are described in the legend.

The value found for ratio $\mathcal{K}(\Lambda_c) = \mathcal{B}(\Lambda_b \to \Lambda_c\tau\nu_\tau)/\mathcal{B}(\Lambda_b \to \Lambda_c 3\pi)$ is

$$\mathcal{K}(\Lambda_c^+) = 2.46 \pm 0.27\,(\text{stat}) \pm 0.40\,(\text{syst})\,, \tag{14}$$

where the systematic uncertainty is driven by the uncertainty on the template shapes and the double charm backgrounds. The branching fraction of the $\Lambda_b \to \Lambda_c \tau \nu_\tau$ decay is measured to be

$$\mathcal{B}(\Lambda_b \to \Lambda_c \tau \nu_\tau) = (1.50 \pm 0.16\,(\text{stat}) \pm 0.25\,(\text{syst}) \pm 0.23\,(\text{ext}))\%\,, \tag{15}$$

where the latter uncertainty is due to external branching fraction measurements coming from the PDG averages of previous measurements [60]. Finally, ratio $\mathcal{R}(\Lambda_c^+)$ is found to be

$$\mathcal{R}(\Lambda_c^+) = 0.242 \pm 0.026\,(\text{stat}) \pm 0.040\,(\text{syst}) \pm 0.059\,(\text{ext})\,, \tag{16}$$

which is in agreement with the SM within 1σ. The largest uncertainty comes from the uncertainty on the $\Lambda_b^0 \to \Lambda_c^+ 3\pi$ branching fraction.

4.2.2. $\mathcal{R}(J/\psi)$ at LHCb

The last measurement from LHCb presented here studies the ratio in the $B_c \to J/\psi\,\ell\nu_\ell$ decay, with muonic τ decays [61]:

$$\mathcal{R}(J/\psi) = \frac{\mathcal{B}(B_c \to J/\psi\,\tau\nu_\tau)}{\mathcal{B}(B_c \to J/\psi\,\mu\nu_\mu)}\,. \tag{17}$$

This measurement uses the lifetime of the B_c meson as a fit variable. Since this is nearly three times shorter than the lifetime of other b hadrons, this helps to reduce backgrounds from the other b hadrons. In addition, it uses the m^2_{miss} variable and q^2 and E^*_μ combined into variable Z. The eight bins of Z show two times four bins of E^*_μ; the first four correspond to events with $q^2 < 7.15\ \text{GeV}^2$ and the next four to values of $q^2 > 7.15\ \text{GeV}^2$.

The form factors of the $B_c \to J/\psi\,\ell\nu_\ell$ decay, for which there were no precise predictions at the time of the measurement, are also included in the fit. The fit is shown in Figure 8, and the analysis yields a value of

$$\mathcal{R}(J/\psi) = 0.71 \pm 0.17\,(\text{stat}) \pm 0.18\,(\text{syst})\,.$$

One of the largest systematic uncertainties in this measurement is the size of the simulated samples. However, unlike in other analyses, the largest systematic uncertainty comes from the lack of knowledge on the form factors. These have since been updated using lattice calculations [34], such that a future measurement can have reduced systematic uncertainty. These updated form factors also include a new prediction for the value of $\mathcal{R}(J/\psi) = 0.2582(38)$, which makes the LHCb measurement 1.8σ higher than the SM prediction.

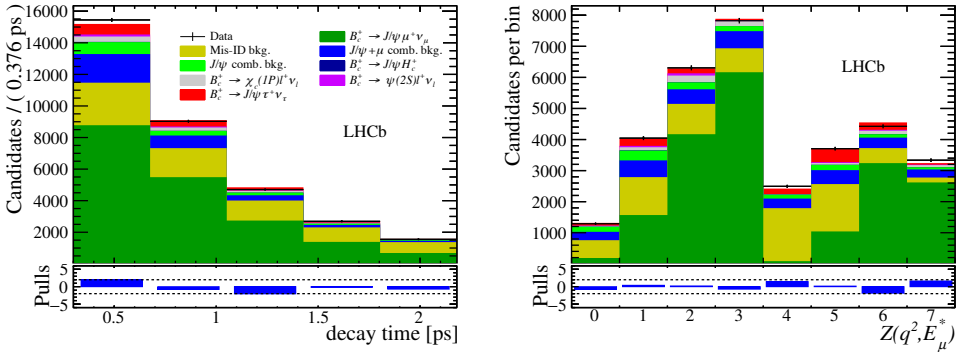

Figure 8. Fit projections of the τ decay time (**left**) and $Z(q^2, E^*_\mu)$ (**right**) variables in the measurement of $\mathcal{R}(J/\psi)$ from LHCb [61].

4.2.3. $\mathcal{R}(J/\psi)$ at CMS

The first CMS measurement of LFU tests in semileptonic $b \to c$ decays is a measurement of $\mathcal{R}(J/\psi)$ [40]. It uses CMS's 2018 dataset of 59.7 fb^{-1} and looks at muonic τ decays. To reconstruct the four-momentum of the B_c^+ meson, this analysis uses the assumption that the momentum of the visible decay products of the B_c^+ is the same as the momentum of the B_c^+ itself, while the mass is the nominal B_c^+ mass.

The fit variables used in this measurement are q^2, combined with IP/σ_{IP} and $L_{xy}/\sigma_{L_{xy}}$, where IP is the impact parameter between the third muon and the J/ψ vertex and L_{xy} is the distance between the beam spot and the J/ψ vertex in the plane transverse to the beam axis. The latter two variables exploit the short B_c^+ lifetime to reduce backgrounds from other B decays. Both of them are divided by their respective uncertainty.

The measurements yield a value of

$$\mathcal{R}(J/\psi) = 0.17^{+0.18}_{-0.17}\,(\text{stat})^{+0.21}_{-0.22}\,(\text{syst})^{+0.19}_{-0.18}\,(\text{ext})\,, \tag{18}$$

which has comparable uncertainties to LHCb's Run 1 measurements and shows good prospects for future analyses with CMS's full dataset. The observed value is in agreement with the SM prediction and with the LHCb measurement.

4.3. Polarization Measurements

4.3.1. D^* Polarization at Belle

As explained in Section 2, measurements of observables beyond the $\mathcal{R}(H_c)$ ratios form a crucial cross-check of the tension with the SM and could provide additional constraints on many new physics scenarios. The Belle experiment shows the first measurement of the fraction of longitudinal polarization of the D^* meson, $F_L^{D^*}$, in semitauonic decays in Ref. [62]. The measurement is based on the inclusive tagging approach. In this approach, the analysis starts from the reconstruction of the signal candidates: a D^0 meson is reconstructed in various decay modes and combined with a charged soft pion to make a D^{*-}, which is then combined with a lepton or a single pion to reconstruct the signal candidate $\overline{B} \to D^*\tau\nu_\tau$ with $\tau \to \ell\nu\nu$ or $\tau \to \pi\nu$. The remaining unassigned charged and neutral particles are all assigned to the tagging side. The invariant mass of the tag side is required to be consistent with the B meson mass. This approach has a higher reconstructed efficiency than the hadronic or semileptonic tagging, but it offers a poor resolution on the kinematics of the signal side. The D^* helicity angle, θ_{hel}, is defined as the angle between the reconstructed D^0 meson and the direction opposite to the B^0 meson in the D^* rest frame. The analysis focuses on region $\theta_{hel} < 0$ because the efficiency to reconstruct the soft pion from the D^* meson for $\theta_{hel} > 0$ is low. The signal is extracted in three bins of θ_{hel}. The fit to the distribution of the helicity angle using Equation (7) offers

$$F_L^{D^*} = 0.60 \pm 0.08\,(\text{stat}) \pm 0.04\,(\text{syst}), \tag{19}$$

which has a total uncertainty dominated by the limited size of the data sample. The largest uncertainty is related to the uncertainty on the model of the $\overline{B} \to D^{**}\tau\nu$ decays. This results in about a 2σ tension with the SM predictions reported in Table 2.

4.3.2. D^* Polarization at LHCb

LHCb's measurement of the D^* polarization [63] in semitauonic decays follows the selection strategy of the hadronic $\mathcal{R}(D^*)$ measurements [56,57] and also looks at three-prong τ decays. It uses the combined dataset of analyses, Run 1 and the 2015–2016 data-taking years of Run 2, and applies very similar selection requirements. The main background from $B \to D^*3\pi$ decays is suppressed by exploiting the displaced decay vertex. The double-charm backgrounds are reduced by the same BDT as described in Ref. [56].

The measurement is performed in two bins of q^2, $q^2 < 7\,\text{GeV}^2$ and $q^2 > 7\,\text{GeV}^2$, which have a similar amount of signal events. The number of q^2 bins can be extended with higher available statistics in the near future. The yields of unpolarized and polarized events are

found through a four-dimensional template fit in bins of t_τ, q^2, $\cos\theta_{hel}$, and the anti-D_s^+ BDT. The fits are performed simultaneously to the Run 1 and Run 2 data sets, and the results of the yields are used to find the following values for the fraction of longitudinal polarization of the D^* meson:

$$F_L^{D^*} = 0.51 \pm 0.07\,(\text{stat}) \pm 0.03\,(\text{syst}), \text{for } q^2 < 7\,\text{GeV}^2, \quad (20)$$

$$F_L^{D^*} = 0.35 \pm 0.08\,(\text{stat}) \pm 0.02\,(\text{syst}), \text{for } q^2 > 7\,\text{GeV}^2, \quad (21)$$

$$F_L^{D^*} = 0.43 \pm 0.06\,(\text{stat}) \pm 0.03\,(\text{syst}), \text{for the full } q^2 \text{ range}. \quad (22)$$

The value obtained for the full q^2 range is compatible with the SM predictions reported in Table 2. Also, the results in the two bins are consistent with the SM. The main systematic uncertainties are due to the limited size of the simulated samples, form factor parameters, and the D_s^+ decay model.

5. Discussion and Interpretations

A summary of the $\mathcal{R}(D)$–$\mathcal{R}(D^*)$ measurements described before and the latest average provided by HFLAV are reported in Table 3 and shown in Figure 9. The average by HFLAV considers the systematic uncertainties due to $B \to D$ and $B \to D^*$ form factors and the contribution from the background due to feed down from $B \to D^{**}\ell\nu$ decays to be fully correlated. This is generally considered a conservative assumption. The p-value of the average is 35%. The experimental average deviates from the HFLAV SM average reported in Table 1 by about 3.3σ, while its deviation from the prediction based on LQCD alone decreases to about 2.5σ.

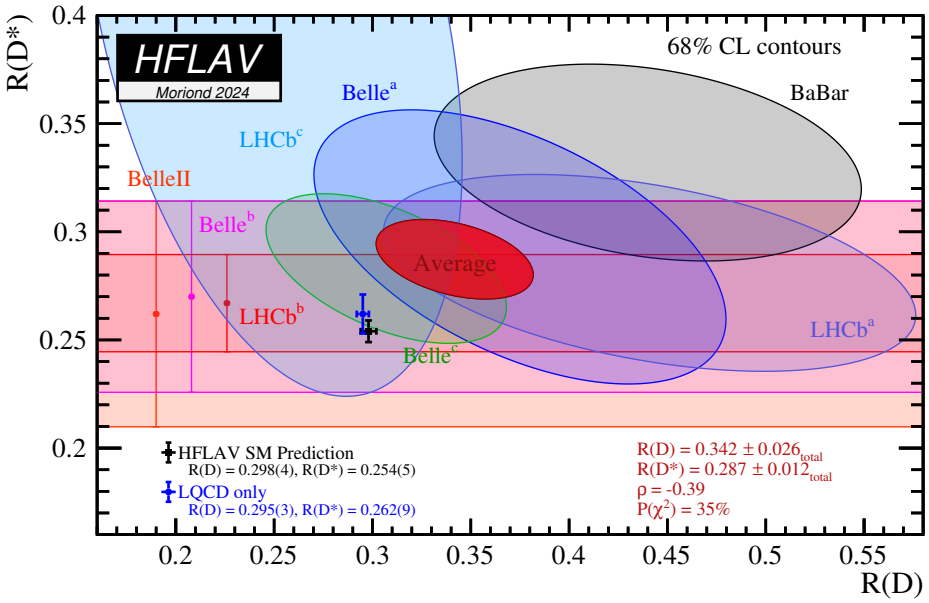

Figure 9. Measurements of $\mathcal{R}(D)$ and $\mathcal{R}(D^*)$ listed in Table 3 and their two-dimensional average. Contours correspond to 68% CL for both the bands and the ellipses. The black and blue points with error bars are two recent SM predictions for $\mathcal{R}(D^*)$ and $\mathcal{R}(D)$. The SM prediction reported is based on the results summarized in Table 1. This prediction and the experimental average deviate from each other by about 3.3σ. The SM prediction based only on LQCD calculations is also reported, where $\mathcal{R}(D)$ is taken from FLAG [25], while $\mathcal{R}(D^*)$ is taken from Ref. [28]. The deviation from the experimental average and this prediction is about 2.5σ. The measurements are listed in Table 3.

It is worth noting that a meta-analysis presented in Ref. [2] shows that the D^{**} contributions in the background involve some significant correlations with $\mathcal{R}(D)$–$\mathcal{R}(D^*)$ measurements. This leads to a larger deviation from the SM prediction. We do not further discuss this observation. Future precise measurements of $\bar{B} \to D^{**}\ell\nu_\ell$ decays, both

concerning the decay rate and the form factors, are pivotal for a reliable estimation of this correlated source of backgrounds.

The observed enhancements of the $\mathcal{R}(D^{(*)})$ ratios relative to the expectations of the SM are persistent, but their significance is not enough to establish a violation of LFU. Moreover, the most recent measurements of these ratios are in reasonable agreement with the SM predictions.

Table 3. Summary of the measurements of $\mathcal{R}(D^*)$ and $\mathcal{R}(D)$, their correlations, and the combined average as obtained by HFLAV [22].

Experiment	$\mathcal{R}(D^*)$	$\mathcal{R}(D)$	ρ
BaBar [42,43]	$0.332 \pm 0.024_{\text{stat}} \pm 0.018_{\text{syst}}$	$0.440 \pm 0.058_{\text{stat}} \pm 0.042_{\text{syst}}$	-0.27
Belle[a] [44]	$0.293 \pm 0.038_{\text{stat}} \pm 0.015_{\text{syst}}$	$0.375 \pm 0.064_{\text{stat}} \pm 0.026_{\text{syst}}$	-0.49
Belle[b] [49]	$0.270 \pm 0.035_{\text{stat}}\,^{+0.028}_{-0.025\,\text{syst}}$		
Belle[c] [48]	$0.283 \pm 0.018_{\text{stat}} \pm 0.014_{\text{syst}}$	$0.307 \pm 0.037_{\text{stat}} \pm 0.016_{\text{syst}}$	-0.51
LHCb[a] [53]	$0.281 \pm 0.018_{\text{stat}} \pm 0.024_{\text{syst}}$	$0.441 \pm 0.060_{\text{stat}} \pm 0.066_{\text{syst}}$	-0.43
LHCb[b] [56,57,64]	$0.267 \pm 0.012_{\text{stat}} \pm 0.019_{\text{syst}}$		
LHCb[c] [54]	$0.402 \pm 0.081_{\text{stat}} \pm 0.085_{\text{syst}}$	$0.249 \pm 0.043_{\text{stat}} \pm 0.047_{\text{syst}}$	-0.39
Belle II [45]	$0.262^{+0.041}_{-0.039\,\text{stat}}{}^{+0.035}_{-0.032\,\text{syst}}$		
Average	$\mathbf{0.287 \pm 0.012}$	$\mathbf{0.342 \pm 0.026}$	-0.39

However, over the last decade, these tensions earned significant attention and led to investigations into new physics models. One proposal involves a new vector boson called W' [65,66], which is similar to the SM W boson but has a coupling that varies between generations of leptons and quarks. This particular model has been ruled out by direct searches at hadron colliders and indirectly by precise measurements of μ and τ decays.

Another potential candidate is the charged Higgs, $H^{\pm}$, as predicted in various extensions of the SM, like the two Higgs Doublet model, 2HDM. This model has been widely discussed in the past, e.g., in Ref. [67,68]. The process with the $H^{\pm}$ boson, shown in Figure 10 (left), interferes with the SM process, producing an enhancement or a depletion of the ratio $\mathcal{R}(D)$ while keeping the ratio $\mathcal{R}(D^*)$ almost unchanged. This model, in its simplest form, has been ruled out because the deviations compared to SM predictions are of the same order for both $\mathcal{R}(D)$ and $\mathcal{R}(D^*)$. Additionally, the q^2 spectra observed by BABAR are also inconsistent with the best fit results obtained from the ratios [42]. However, more general models with charged Higgs bosons can still explain the observed tensions [69].

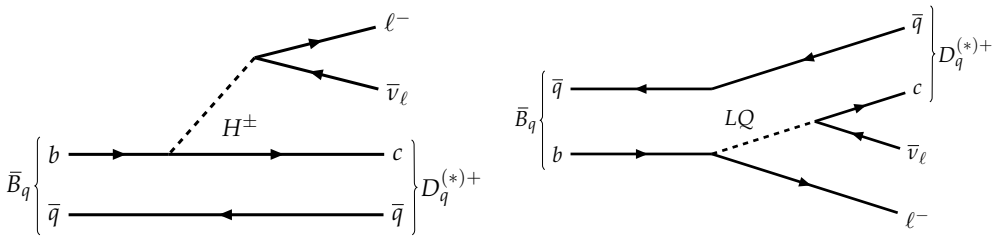

Figure 10. Diagrams of the $\overline{B}_q \to D_q^{(*)+}\ell^-\overline{\nu}_\ell$ decay for a process mediated (**left**) by a hypothetical spin-0 charged Higgs boson ($H^{\pm}$) or (**right**) coupling to a leptoquark (LQ).

There is a possibility that the deviation could be attributed to leptoquarks (LQs). There has been extensive discussion on this topic in the literature; a recent review can be found in Ref. [70]. A lowest-order diagram describing B meson decays mediated by a LQ is shown in Figure 10 (right). However, explaining the deviation with LQs requires making some ad hoc assumptions to avoid constraints from direct searches, some of which have been carried out at the LHC [71,72] and other indirect constrains. Recently, it was shown in Ref. [70] that some LQ models predict strong correlations between $b \to c\tau\nu_\tau$ and $\Upsilon(nS) \to \tau\tau$ decays. The measurement of ratio $\mathcal{B}(\Upsilon(3S) \to \tau^+\tau^-)/\mathcal{B}(\Upsilon(3S) \to \ell^+\ell^-)$ obtained by BABAR [73]

is consistent with the SM prediction, allowing to put stringent limits on the couplings of these LQ models.

The interpretation of the measured values of the ratios in terms of the new physics model has some limitations. The measurements of the $\mathcal{R}(H_c)$ ratios are carried out based on the SM for the signal templates. For this reason, it is not always straightforward to use the published results assuming the SM to put constraints on specific new physics models. This was demonstrated in Ref. [42] by BABAR and in Ref. [49] by Belle, where it was shown that the shape of signal templates, as a function of, e.g., m^2_{miss} or p_ℓ, needed to extract the signal yield, as well as efficiency ratio $\epsilon_{norm}/\epsilon_{sig}$ in Equation (11), which are significantly influenced by the parameters of the model under consideration. Therefore, determining the compatibility of the data with specific new physics models requires refitting of the data with signal templates consistent with the model considered.

Because of this embedded model dependence in the study of semitauonic decays, it is currently unclear how experiments could provide enough information to ensure a reliable reinterpretation of the analysis results. A robust approach would be for experiments to perform analyses that fit a large portion of the possible new physics couplings in a multidimensional space. To achieve this, many simulation samples are required for each point in the space of new physics couplings. This can be accomplished by reweighing existing MC samples instead of generating multiple simulations. This approach led a group of theorists and experimentalists to develop HAMMER [30], a software tool which enables the reweighting of the MC samples for a wide range of decay modes and new physics couplings.

Additionally, it cannot be ruled out that the theoretical predictions may not be as reliable as currently assumed. We already showed in Section 2 that there are some tensions in the most recent predictions for $\mathcal{R}(D^*)$ based on LQCD and the most recent data. These tensions require additional studies from both the theory and experimental side.

It was noted in Ref. [74] that QED corrections depend non-trivially on the lepton mass and do not cancel in the $\mathcal{R}(H_c)$ ratios. These contributions are well approximated in the experimental simulation by PHOTOS [75], but some are neglected. The Coulomb-term correction, as shown in Ref. [76], may eventually become important. This term causes isospin breaking due to its different contributions in $\mathcal{R}(D^0)$ and $\mathcal{R}(D^+)$. Generally, the QED contributions are anticipated to be minor, but they might become significant when measurements are performed with greater precision.

6. Summary and Outlook

The existing experimental results on semitauonic decays are limited by the size of the available data samples, the uncertainties in the reconstruction efficiencies, and the background estimates. The various experiments are continuing their analysis efforts to improve their methods and obtain more accurate and reliable results. Belle and BABAR analyzed their full dataset. While Belle provided many measurements with different analysis approaches using their full dataset, BABAR published a single measurement, which is the one that deviates most from the SM. It would be interesting to reanalyze the BABAR data using different B-tagging algorithms and to take advantage of the enhanced understanding of certain backgrounds and the signal model.

Many analyses are ongoing by the Belle II and LHCb experiments. The status in the middle of 2024 is that Belle II is currently collecting data at the nominal luminosity, while LHCb is in the commissioning phase after it underwent a major upgrade in the recent years. In the next years, both experiments will collect enough data to reduce the statistical uncertainty on most of their measurements to the level of a few percent. It is expected that most of the systematic uncertainties on the $\mathcal{R}(H_c)$ ratios can be reduced with the increase in the data sample because most of these are related to the size of the control samples extracted from the data.

We do not provide projections on expected uncertainties with the future data. These extrapolations, while interesting and useful for long-term plans, are based on many as-

sumptions that are usually broken by the development of improved analysis techniques. A study of expected uncertainties as a function of the luminosity for various measurements of $\mathcal{R}(H_c)$ ratios, for both LHCb and Belle II, was reported in Ref. [30]. The researchers are working hard to improve the measurements of semitauonic decays by refining their methods, enhancing signal samples, improving efficiencies, and examining all aspects of the signal extraction. In the following, we illustrate the future directions of these important measurements in general terms.

Belle II has already collected a larger data sample than the one used in Ref. [45], and it is currently taking data. We expect many new measurements of B^0 and B^+ decays to be derived from these data. The upcoming larger sample will allow for more precise measurements based on detailed studies of their kinematics. Studies of the full angular and q^2 distributions, as well as the tau polarization, will offer much additional information. Belle II will also probe semitauonic $b \to u$ decays. At present, only an upper limit for $\bar{B} \to \pi\tau\nu_\tau$ exists [77], but with more data, this and other similar channels should be accessible at Belle II.

Most of the measurements performed by LHCb are based only on part of the available dataset. At present, LHCb is collecting data with a higher instantaneous luminosity compared to Run 1 and Run 2. The enhanced trigger selection and data rate capability allow a larger efficiency for most of the b-hadron decay modes of interest. LHCb has already shown its capability to perform studies of angular distributions in $B \to D^{(*)}\ell\nu$ decays, with the measurement of the D^* longitudinal polarization fraction. Other angular distributions can be studied with hadronic τ decays, which offer a better resolution compared to muonic τ decays.

Given the high production rate of B_s and B_c mesons and various b-baryons, LHCb is planning an extensive program to measure their semileptonic branching fractions, form factors, and to search for deviations from SM expectations. Even if the tension in $\mathcal{R}(D)$ and $\mathcal{R}(D^*)$ reduce in the future, the studies of LFU with additional kinds of b-hadrons will help to constrain many kinds of new physics. For instance, $\bar{B}_s \to D_s^{(*)}\tau\nu_\tau$ decays, which probe the same interaction as $\bar{B} \to D^{(*)}\ell\nu_\ell$ decays, are affected by different sources of background due to the huge differences between the D^{**} and D_s^{**} spectroscopy. CMS has also shown that, for some channels like $B_c \to J/\psi\tau\nu_\tau$ with three leptons in the final state, it can provide interesting and complementary measurements. The parked data still need to be fully exploited by CMS.

In the near future, it will be important to extend the LFU searches to measurements of other observables, like asymmetries in the angular distributions, and the precise measurements of the spectrum of the final-state kinematics. At present, only the polarization of the D^* and the τ lepton have been determined. The D^* longitudinal polarization is the easiest to determine at both Belle II and LHCb. The τ polarization has been determined by Belle using τ decays into a single pion, which is the ideal process to access the τ polarization. At LHCb, this measurement could be carried out using a sample with $\tau \to 3\pi\nu$ decays, but the sensitivity will be much reduced and very large samples would be required to reach a significant sensitivity.

Future improvements can be achieved only if some critical ancillary measurements are performed by both Belle II and LHCb. Here is a list of some of these measurements:

1. Detailed studies of $\bar{B} \to D^{**}\ell\nu_\ell$ decays, which will provide the first measurements of $\mathcal{R}(D^{**})$, will result in a significant reduction in uncertainties in estimating this background for measurements of $\bar{B} \to D^{(*)}\ell\nu_\ell$ decays.
2. The current understanding of double-charmed decays of b hadrons of the type $H_b \to H_c^{'} H_c^{''} X$ is also quite limited. Although both the B factories and LHCb have appropriate control decay modes to constrain this background from data, additional measurements are required to decrease the uncertainties caused by the decay models for these types of backgrounds. This is particularly important for LHCb, which cannot provide a clean tagging of b hadrons.

3. Both LHCb and Belle II will be essential to improve the knowledge of the form factors for various semileptonic b-hadron decays. The relevance of precise studies of semileptonic decays of c hadrons should not be underestimated either. BESIII will be the major experiment to provide form factors and branching fraction measurements for most of the c hadrons.

In conclusion, we anticipate that in the future we will have numerous interesting measurements of semitauonic decays of b hadrons from Belle II, LHCb, and possibly CMS. This will determine whether the observed anomalies are genuine or if they are the result of systematic underestimation or unfortunate statistical fluctuation. Confirmation of deviations from Standard Model predictions would strongly suggest the presence of contributions from new physics.

Author Contributions: Both authors have equally contributed. All authors have read and agreed to the published version of the manuscript.

Funding: This publication is part of the project *Uncovering the lepton generation gap* (with project number VI.Veni.202.004 of the research programme Veni which is partly financed by the Dutch Research Council (NWO)). The work of M.R. is supported in part by the Italian Ministry of Research (MUR) under the grant PRIN 2022N4W8WR.

Conflicts of Interest: The authors declare no conflicts of interest.

References

1. Ciezarek, G.; Franco Sevilla, M.; Hamilton, P.M.; Kowalewski, R.; Kuhr, T.; Lüth, V.; Sato, Y. A challenge to lepton universality in B meson decays. *Nature* **2017**, *546*, 227–233 . [CrossRef] [PubMed]
2. Bernlochner, F.U.; Sevilla, M.F.; Robinson, D.J.; Wormser, G. Semitauonic b-hadron decays: A lepton flavor universality laboratory. *Rev. Mod. Phys.* **2022**, *94*, 015003. [CrossRef]
3. Ricciardi, G.; Rotondo, M. Determination of the Cabibbo-Kobayashi-Maskawa matrix element $|V_{cb}|$. *J. Phys. G* **2020**, *47*, 113001. [CrossRef]
4. Gambino, P.; Kronfeld, A.S; Rotondo, M; Schwanda, C.; Bernlochner, F.; Bharucha, A.; Bozzi, C.; Calvi, M.; Cao, L. and Ciezarek, G.; et al. Challenges in semileptonic B decays. *Eur. Phys. J. C* **2020**, *80*, 966. [CrossRef]
5. Richman, J.D.; Burchat, P.R. Leptonic and semileptonic decays of charm and bottom hadrons. *Rev. Mod. Phys.* **1995**, *67*, 893–976. [CrossRef]
6. Hagiwara, K.; Martin, A.D.; Wade, M.F. Exclusive semileptonic B meson decays. *Nucl. Phys. B* **1989**, *327*, 569–594. [CrossRef]
7. Bigi, D.; Gambino, P. Revisiting $B \to D\ell\nu$. *Phys. Rev. D* **2016**, *94*, 094008. [CrossRef]
8. Sirlin, A. Large m_W, m_Z behavior of the $O(\alpha)$ corrections to semileptonic processes mediated by W. *Nucl. Phys. B* **1982**, *196*, 83–92. [CrossRef]
9. Fermilab Lattice and MILC Collaborations. Semileptonic form factors for $B \to D^*\ell\nu$ at nonzero recoil from $2+1$-flavor lattice QCD: Fermilab Lattice and MILC Collaborations. *Eur. Phys. J. C* **2022**, *82*, 1141; Erratum in *Eur. Phys. J. C* **2023**, *83*, 21. [CrossRef]
10. Harrison, J.; Davies, C.T.H. $B \to D^*$ and $B_s^0 \to D_s^*$ vector, axial-vector and tensor form factors for the full q^2 range from lattice QCD. *Phys. Rev. D* **2024**, *109*, 094515. [CrossRef]
11. Aoki, Y.; Colquhoun, B.; Fukaya, H.; Hashimoto, S.; Kaneko, T.; Kellermann, R.; Koponen, J.; Kou, E. $B \to D^*\ell\nu_\ell$ semileptonic form factors from lattice QCD with Möbius domain-wall quarks. *Phys. Rev. D* **2024**, *109*, 074503. [CrossRef]
12. Caprini, I.; Lellouch, L.; Neubert, M. Dispersive bounds on the shape of $\bar{B} \to D^{(*)}\ell\bar{\nu}$ form-factors. *Nucl. Phys. B* **1998**, *530*, 153–181. [CrossRef]
13. Boyd, C.G.; Grinstein, B.; Lebed, R.F. Model-independent extraction of $|V_{cb}|$ using dispersion relations. *Phys. Lett. B* **1995**, *353*, 306–312. [CrossRef]
14. Bourrely, C.; Caprini, I.; Lellouch, L. Model-independent description of $B \to \pi\ell\nu$ decays and a determination of $|V_{ub}|$. *Phys. Rev. D* **2009**, *79*, 013008; Erratum in *Phys. Rev. D* **2010**, *82*, 099902. [CrossRef]
15. Colangelo, P.; De Fazio, F. Scrutinizing $\bar{B} \to D^*(D\pi)\ell^-\bar{\nu}_\ell$ and $\bar{B} \to D^*(D\gamma)\ell^-\bar{\nu}_\ell$ in search of new physics footprints. *J. High Energy Phys.* **2018**, *6*, 82. [CrossRef]
16. Martinelli, G.; Simula, S.; Vittorio, L. $|V_{cb}|$ and $\mathcal{R}(D^{(*)})$ using lattice QCD and unitarity. *Phys. Rev. D* **2022**, *105*, 034503. [CrossRef]
17. Gambino, P.; Jung, M.; Schacht, S. The V_{cb} puzzle: An update. *Phys. Lett.* **2019**, *B795*, 386–390. [CrossRef]
18. Bordone, M.; Jung, M.; van Dyk, D. Theory determination of $\bar{B} \to D^{(*)}\ell^-\bar{\nu}$ form factors at $\mathcal{O}(1/m_c^2)$. *Eur. Phys. J. C* **2020**, *80*, 74. [CrossRef]
19. Bernlochner, F.U.; Ligeti, Z.; Papucci, M.; Robinson, D.J. Combined analysis of semileptonic B decays to D and D^*: $\mathcal{R}(D^{(*)})$, $|V_{cb}|$, and new physics. *Phys. Rev. D* **2017**, *95*, 115008; Erratum in *Phys. Rev. D* **2018**, *97*, 059902. [CrossRef]

20. Jaiswal, S.; Nandi, S.; Patra, S.K. Extraction of $|V_{cb}|$ from $B \to D^{(*)}\ell\nu_\ell$ and the Standard Model predictions of $\mathcal{R}(D^{(*)})$. *J. High Energy Phys.* **2017**, *12*, 060. [CrossRef]
21. BABAR Collaboration. Extraction of form factors from a four-dimensional angular analysis of $\bar{B} \to D^*\ell^-\bar{\nu}_\ell$. *Phys. Rev. Lett.* **2019**, *123*, 091801. [CrossRef] [PubMed]
22. HFLAV Collaboration. Averages of b-hadron, c-hadron, and τ-lepton properties as of 2021. *Phys. Rev. D* **2023**, *107*, 052008. [CrossRef]
23. Bigi, D.; Gambino, P.; Schacht, S. $\mathcal{R}(D^*)$, $|V_{cb}|$, and the Heavy Quark Symmetry relations between form factors. *J. High Energy Phys.* **2017**, *11*, 61. [CrossRef]
24. Bernlochner, F.U.; Ligeti, Z.; Papucci, M.; Prim, M.T.; Robinson, D.J.; Xiong, C. Constrained second-order power corrections in HQET: $\mathcal{R}(D^*)$, $|V_{cb}|$, and new physics. *Phys. Rev. D* **2022**, *106*, 096015. [CrossRef]
25. Flavour Lattice Averaging Group (FLAG) Collaboration. FLAG Review 2021. *Eur. Phys. J. C* **2022**, *82*, 869. [CrossRef]
26. Martinelli, G.; Simula, S.; Vittorio, L. Exclusive determinations of $|V_{cb}|$ and $\mathcal{R}(D^*)$ through unitarity. *Eur. Phys. J. C* **2022**, *82*, 1083. [CrossRef]
27. Ray, I.; Nandi, S. Test of new physics effects in $\bar{B} \to \left(D^{(*)}, \pi\right)\ell^-\bar{\nu}_\ell$ decays with heavy and light leptons. *J. High Energy Phys.* **2024**, *1*, 22. [CrossRef]
28. Martinelli, G.; Simula, S.; Vittorio, L. Updates on the determination of $|V_{cb}|$, $\mathcal{R}(D^*)$ and $|V_{ub}|/|V_{cb}|$. *Eur. Phys. J. C* **2024**, *84*, 400. [CrossRef]
29. Bordone, M.; Juttner, A. New strategies for probing $B \to D^*\ell\bar{\nu}_\ell$ lattice and experimental data. *arXiv* **2024**, arXiv:2406.10074.
30. Bernlochner, F.U.; Duell, S.; Ligeti, Z.; Papucci, M.; Robinson, D.J. Das ist der HAMMER: Consistent new physics interpretations of semileptonic decays. *Eur. Phys. J. C* **2020**, *80*, 883. [CrossRef]
31. Bernlochner, F.U.; Ligeti, Z.; Robinson, D.J.; Sutcliffe, W.L. Precise predictions for $\Lambda_b \to \Lambda_c$ semileptonic decays. *Phys. Rev. D* **2019**, *99*, 055008. [CrossRef]
32. Detmold, W.; Lehner, C.; Meinel, S. $\Lambda_b \to p\ell^-\bar{\nu}_\ell$ and $\Lambda_b \to \Lambda_c\ell^-\bar{\nu}_\ell$ form factors from lattice QCD with relativistic heavy quarks. *Phys. Rev. D* **2015**, *92*, 034503. [CrossRef]
33. LHCb Collaboration. Measurement of the shape of the $\Lambda_b^0 \to \Lambda_c^+\mu^-\bar{\nu}_\mu$ differential decay rate. *Phys. Rev. D* **2017**, *96*, 112005. [CrossRef]
34. Harrison, J.; Davies, C.T.H.; Lytle, A. $R(J/\psi)$ and $B_c^- \to J/\psi\ell^-\bar{\nu}_\ell$ lepton flavor universality violating observables from lattice QCD. *Phys. Rev. Lett.* **2020**, *125*, 222003. [CrossRef] [PubMed]
35. Feindt, M.; Keller, F.; Kreps, M.; Kuhr, T.; Neubauer, S.; Zander, D.; Zupanc, A. A hierarchical NeuroBayes-based algorithm for full reconstruction of B mesons at B factories. *Nucl. Instrum. Meth. A* **2011**, *654*, 432–440. [CrossRef]
36. Nason, P.; Ridolfi, G.; Schneider, O.; Tartarelli, G.; Vikas, P.; Baines, J.; Baranov, S.; Bartalini, P.; Bay, A.; Bouhova, E.; et al. Bottom production. In Proceedings of the Workshop on Standard Model Physics (and More) at the LHC (First Plenary Meeting), Geneva, Switzerland, 25–26 May 1999 ; pp. 231–304. [CrossRef]
37. LHCb Collaboration. The LHCb detector at the LHC. *JINST* **2008**, *3*, S08005. [CrossRef]
38. LHCb Collaboration. Measurement of the b-quark production cross-section in 7 and 13 TeV pp collisions. *Phys. Rev. Lett.* **2017**, *118*, 052002; Erratum in *Phys. Rev. Lett.* **2017**, *119*, 169901. [CrossRef] [PubMed]
39. LHCb Collaboration. LHCb detector performance. *Int. J. Mod. Phys. A* **2015**, *30*, 1530022. [CrossRef]
40. CMS Collaboration; Test of Lepton Flavor Universality Violation in Semileptonic B_c^+ Meson Decays at CMS. CMS-PAS-BPH-22-012. 2023. Available online: https://cds.cern.ch/record/2868988 (accessed on 1 July 2024).
41. LHCb Collaboration. Measurement of the ratio of branching fractions $\mathcal{B}(\bar{B}^0 \to D^{*+}\tau^-\bar{\nu}_\tau)/\mathcal{B}(\bar{B}^0 \to D^{*+}\mu^-\bar{\nu}_\mu)$. *Phys. Rev. Lett.* **2015**, *115*, 111803; Erratum in *Phys. Rev. Lett.* **2015**, *115*, 159901. [CrossRef] [PubMed]
42. BABAR Collaboration. Evidence for an excess of $\bar{B} \to D^{(*)}\tau^-\bar{\nu}_\tau$ decays . *Phys. Rev. Lett.* **2012**, *109*, 101802. [CrossRef]
43. BABAR Collaboration. Measurement of an excess of $\bar{B} \to D^{(*)}\tau^-\bar{\nu}_\tau$ decays and implications for charged Higgs bosons . *Phys. Rev. D* **2013**, *88*, 072012. [CrossRef]
44. Belle Collaboration. Measurement of the branching ratio of $\bar{B} \to D^{(*)}\tau^-\bar{\nu}_\tau$ relative to $\bar{B} \to D^{(*)}\ell^-\bar{\nu}_\ell$ decays with hadronic tagging at Belle . *Phys. Rev. D* **2015**, *92*, 072014. [CrossRef]
45. Belle II Collaboration. A test of lepton flavor universality with a measurement of $\mathcal{R}(D^*)$ using hadronic B tagging at the Belle II experiment. *arXiv* **2024**, arXiv:2401.02840.
46. Keck, T.; Abudinén, F.; Bernlochner, F.; Cheaib, R.; Cunliffe, S.; Feindt, M.; Ferber, T.; Gelb, M.; Gemmler, J.; Goldenzweig, P.; et al. The Full Event Interpretation: An exclusive tagging algorithm for the Belle II experiment. *Comput. Softw. Big Sci.* **2019**, *3*, 6. [CrossRef]
47. Belle Collaboration. Measurement of the branching ratio of $\bar{B}^0 \to D^{*+}\tau^-\bar{\nu}_\tau$ relative to $\bar{B}^0 \to D^{*+}\ell^-\bar{\nu}_\ell$ decays with a semileptonic tagging method. *Phys. Rev. D* **2016**, *94*, 072007. [CrossRef]
48. Belle Collaboration. Measurement of $\mathcal{R}(D)$ and $\mathcal{R}(D^*)$ with a semileptonic tagging method. *Phys. Rev. Lett.* **2020**, *124*, 161803. [CrossRef] [PubMed]
49. Belle Collaboration. Measurement of the τ lepton polarization and $\mathcal{R}(D^*)$ in the decay $\bar{B} \to D^*\tau^-\bar{\nu}_\tau$. *Phys. Rev. Lett.* **2017**, *118*, 211801. [CrossRef] [PubMed]
50. Belle Collaboration. Measurement of the τ lepton polarization and $R(D^*)$ in the decay $\bar{B} \to D^*\tau^-\bar{\nu}_\tau$ with one-prong hadronic τ decays at Belle. *Phys. Rev. D* **2018**, *97*, 012004. [CrossRef]

51. Belle II Collaboration. First measurement of $\mathcal{R}(X_{\tau/\ell})$ as an inclusive test of the $b \to c\tau\nu$ anomaly. *Phys. Rev. Lett.* **2024**, *132*, 211804. [CrossRef].
52. Rahimi, M.; Vos, K.K. Standard Model predictions for lepton flavour universality ratios of inclusive semileptonic *B* decays. *J. High Energy Phys.* **2022**, *11*, 7. [CrossRef]
53. LHCb Collaboration. Measurement of the ratios of branching fractions $\mathcal{R}(D^*)$ and $\mathcal{R}(D^0)$. *Phys. Rev. Lett.* **2023**, *131*, 111802. [CrossRef]
54. LHCb Collaboration. Measurement of the branching fraction ratios $\mathcal{R}(D^+)$ and $\mathcal{R}(D^{*+})$ using muonic τ decays. *arXiv* **2024**, arXiv:2406.03387.
55. García Pardiñas, J.; Meloni, S.; Grillo, L.; Owen, P.; Calvi, M.; Serra, N. RooHammerModel: interfacing the HAMMER software tool with HistFactory and RooFit. *JINST* **2022**, *17*, T04006. [CrossRef]
56. LHCb Collaboration. Test of lepton flavor universality using $B^0 \to D^{*-}\tau^+\nu_\tau$ decays with hadronic τ channels. *Phys. Rev. D* **2023**, *108*, 012018; Erratum in *Phys. Rev. D* **2024**, *109*, 119902. [CrossRef]
57. LHCb Collaboration. Test of lepton flavor universality by the measurement of the $B^0 \to D^{*-}\tau^+\nu_\tau$ branching fraction using three-prong τ decays. *Phys. Rev.* **2018**, *D97*, 072013. [CrossRef]
58. Datta, A.; Kamali, S.; Meinel, S.; Rashed, A. Phenomenology of $\Lambda_b \to \Lambda_c\tau\bar{\nu}_\tau$ using lattice QCD calculations. *J. High Energy Phys.* **2017**, *8*, 131. [CrossRef]
59. LHCb Collaboration. Observation of the decay $\Lambda_b^0 \to \Lambda_c^+\tau^-\bar{\nu}_\tau$. *Phys. Rev. Lett.* **2022**, *128*, 191803. [CrossRef] [PubMed]
60. Particle Data Group. Review of particle physics. *PTEP* **2020**, *2020*, 083C01. [CrossRef]
61. LHCb Collaboration. Measurement of the ratio of branching fractions $\mathcal{B}(B_c^+ \to J/\psi\tau^+\nu_\tau)/\mathcal{B}(B_c^+ \to J/\psi\mu^+\nu_\mu)$. *Phys. Rev. Lett.* **2018**, *120*, 121801. [CrossRef]
62. Belle Collaboration. Measurement of the D^{*-} polarization in the decay $B^0 \to D^{*-}\tau^+\nu_\tau$. In Proceedings of the 10th International Workshop on the CKM Unitarity Triangle, Heidelberg, Germany, 17–21 September 2018
63. LHCb Collaboration. Measurement of the D^* longitudinal polarization in $B^0 \to D^{*-}\tau^+\nu_\tau$ decays. *arXiv* **2023**, arXiv:2311.05224.
64. LHCb Collaboration. Measurement of the ratio of the $B^0 \to D^{*-}\tau^+\nu_\tau$ and $B^0 \to D^{*-}\mu^+\nu_\mu$ branching fractions using three-prong τ-lepton decays. *Phys. Rev. Lett.* **2018**, *120*, 171802. [CrossRef] [PubMed]
65. Asadi, P.; Buckley, M.R.; Shih, D. It's all right(-handed neutrinos): A new W' model for the $\mathcal{R}(D^{(*)})$ anomaly. *J. High Energy Phys.* **2018**, *9*, 10. [CrossRef]
66. Greljo, A.; Robinson, D.J.; Shakya, B.; Zupan, J. $\mathcal{R}(D^{(*)})$ from W' and right-handed neutrinos. *J. High Energy Phys.* **2018**, *9*, 169. [CrossRef]
67. Korner, J.G.; Schuler, G.A. Exclusive semileptonic heavy meson decays including lepton mass effects. *Z. Phys. C* **1990**, *46*, 93. [CrossRef]
68. Tanaka, M. Charged Higgs effects on exclusive semitauonic *B* decays. *Z. Phys. C* **1995**, *67*, 321–326. [CrossRef]
69. Datta, A.; Duraisamy, M.; Ghosh, D. Diagnosing new physics in $b \to c\tau\nu_\tau$ decays in the light of the recent BaBar result. *Phys. Rev. D* **2012**, *86*, 034027. [CrossRef]
70. Iguro, S.; Kitahara, T.; Watanabe, R. Global fit to $b \to c\tau\nu$ anomaly 2024 Spring breeze. *arXiv* **2022**, arXiv:2210.10751.
71. ATLAS Collaboration. Search for third generation scalar leptoquarks in pp collisions at $\sqrt{s} = 7$ TeV with the ATLAS detector. *J. High Energy Phys.* **2013**, *6*, 33. [CrossRef]
72. CMS Collaboration. Search for a singly produced third-generation scalar leptoquark decaying to a τ lepton and a bottom quark in proton-proton collisions at $\sqrt{s} = 13$ TeV. *J. High Energy Phys.* **2018**, *7*, 115. [CrossRef]
73. BaBar Collaboration. Precision measurement of the $\mathcal{B}(\Upsilon(3S) \to \tau^+\tau^-)/\mathcal{B}(\Upsilon(3S) \to \mu^+\mu^-)$ ratio. *Phys. Rev. Lett.* **2020**, *125*, 241801. [CrossRef] [PubMed]
74. de Boer, S.; Kitahara, T.; Nisandzic, I. Soft-photon corrections to $\bar{B} \to D\tau^-\bar{\nu}_\tau$ relative to $\bar{B} \to D\mu^-\bar{\nu}_\mu$. *Phys. Rev. Lett.* **2018**, *120*, 261804. [CrossRef]
75. Barberio, E.; Was, Z. PHOTOS: A universal Monte Carlo for QED radiative corrections. Version 2.0. *Comput. Phys. Commun.* **1994**, *79*, 291–308. [CrossRef]
76. Calí, S.; Klaver, S.; Rotondo, M.; Sciascia, B. Impacts of radiative corrections on measurements of lepton flavour universality in $B \to D\ell\nu_\ell$ decays. *Eur. Phys. J. C* **2019**, *79*, 744. [CrossRef]
77. Belle Collaboration. Search for $B^0 \to \pi^-\tau^+\nu_\tau$ with hadronic tagging at Belle. *Phys. Rev. D* **2016**, *93*, 032007. [CrossRef]